American Journal of Interdisciplinary Studies
Volume 03, Issue 03 (2022)
Page No: 36 – 67
eISSN: 3067-5146
Doi: 10.63125/xytn3e23

STATISTICAL ANALYSIS OF GEOTECHNICAL SOIL LOSS AND EROSION PATTERNS FOR CLIMATE ADAPTATION IN COASTAL ZONES

Md. Mominul Haque[1]; Masud Rana[2]; Md. Milon Mia[3];

[1]. *Bachelor's in Civil Engineering, Hubei University of Technology, Hubei, China;*
Email: mominkhan789456@gmail.com
[2]. *BSc in Civil Engineering, Stamford University Bangladesh, Dhaka, Bangladesh;*
Email: masudranasub97@gmail.com
[3]. *Bachelor of Science in Civil Engineering, European University of Bangladesh, Dhaka, Bangladesh*
Email: milon674457@gmail.com

ABSTRACT

This study addresses the pressing problem of quantifying geotechnical soil loss and shoreline erosion in coastal zones under contemporary hydro-climatic forcing, where planners need defensible evidence to design adaptation. The purpose is to explain spatial patterns of erosion by linking measurable substrate properties, exposure regimes, and land cover to decision-relevant outcomes. Using a geological-survey based, quantitative, cross-sectional, multi-case design, we analyzed four contrasting coastal cases instrumented with 76 shore-perpendicular transects, 380 laboratory soil tests, high-precision GNSS and GIS/remote-sensing products, hydro-meteorological reanalysis, and a parallel stakeholder survey of 418 respondents. A structured literature review of 64 peer-reviewed papers scoped variables and hypotheses. The sample comprised open sandy beaches, dune-backed barriers, marsh edges, and scarped bluffs. Key variables included erosion rate and a soil-loss index as outcomes, with predictors spanning runup proxies, significant wave height, rainfall intensity, vegetation cover, cohesion, median grain size, slope, and engineered defenses. The preregistered analysis plan progressed from data auditing, descriptives, and correlation screening to fixed-effects regression with cluster-robust inference, moderation tests, and robustness via GLM (Gamma/log), spatial error models, penalization, and quantile regression. Headline findings show runup exposure as the strongest positive correlate of erosion, rainfall intensity as a secondary contributor, and vegetation cover and soil cohesion as protective; critically, a negative Runup × Vegetation interaction indicates that vegetation buffers exposure effects. Upper-tail losses are disproportionately sensitive to exposure, slope, and substrate resistance. Implications include operational runup-aware monitoring, prioritization of nature-based measures where accommodation and supply permit, preservation of cohesive toes on bluffed coasts, and risk-tiered setbacks calibrated to directional exposure and morphology. Keywords: coastal erosion, soil loss, geological survey, cross-sectional analysis, vegetation buffering, runup exposure, cohesion, nature-based adaptation, spatial modeling, climate risk.

KEYWORDS

Coastal Erosion; Soil Loss; Shoreline Change; Geological Survey; Quantitative Cross-Sectional Design;

Citation:
Haque, M. M., Rana, M., & Mia, M. (2022). *Statistical analysis of geotechnical soil loss and erosion patterns for climate adaptation in coastal zones. American Journal of Interdisciplinary Studies, 3*(3), 36–67.
https://doi.org/10.63125/xytn3e23

Received:
June 18, 2022

Revised:
July 24, 2022

Accepted:
August 26, 2022

Published:
September 07, 2022

Copyright:

© 2022 by the author. This article is published under the license of *American Scholarly Publishing Group Inc* and is available for open access.

American Journal of Interdisciplinary Studies
Volume 03, Issue 03 (2022)
Page No: 36 – 67
eISSN: 3067-0470
DOI: 10.63125/xytn3e23

INTRODUCTION

Coastal erosion is commonly defined as the landward retreat of the shoreline caused by the net removal of sediment from beaches, dunes, bluffs, or cliffs by hydrodynamic forces such as waves, currents, tides, and storm surges acting on materials whose resistance is governed by geotechnical properties (e.g., grain size, cohesion, and shear strength). In geotechnical terms, soil loss reflects the detachment and transport of soil particles driven by hydraulic shear, raindrop impact, and overland or concentrated flow, modulated by intrinsic soil characteristics and vegetation cover. Internationally, the significance of coastal erosion and soil loss is rising because more than one-third of global coastlines are sandy and socioeconomically valuable while being highly dynamic and vulnerable to sea-level rise and changing storm regimes (Nicholls & Cazenave, 2010; Vousdoukas et al., 2020).

Figure 1: integrated geotechnical, hydro-climatic influencing coastal erosion

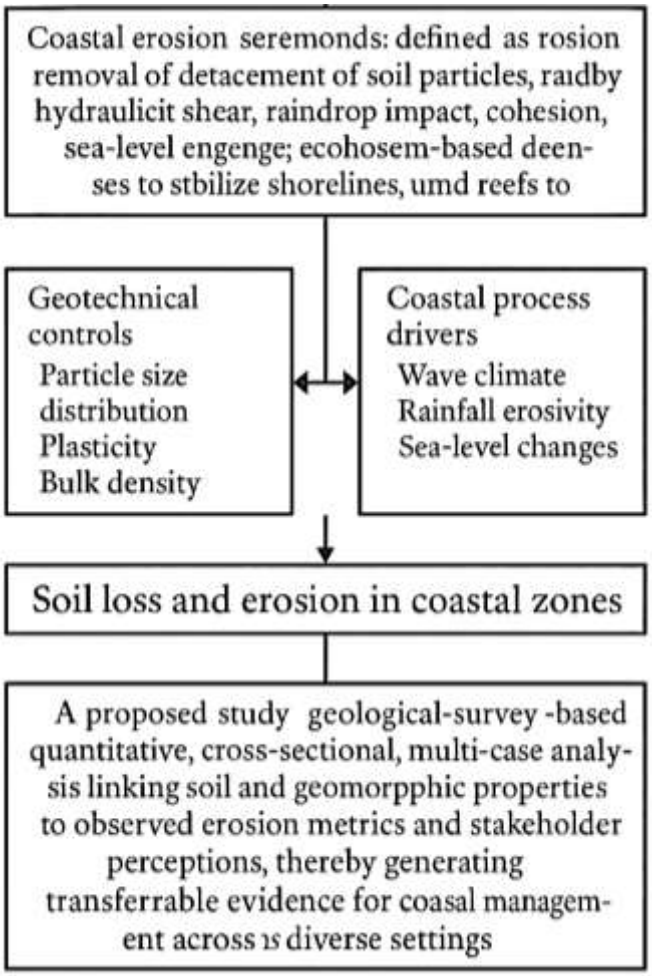

These hazards threaten densely populated deltas, tourist economies, transport infrastructure, and critical ecosystems that provide coastal protection services. Projections suggest that extreme sea levels will occur more frequently this century and that many sandy shorelines could experience chronic retreat without effective adaptation (Hinkel et al., 2014; Muis et al., 2018). At the same time, the scientific and policy communities are increasingly attentive to "nature-based" or "ecosystem-based" defenses, which complement or substitute hard structures by harnessing dunes, marshes, mangroves, and reefs to attenuate waves and stabilize shorelines (Narayan et al., 2016; Shepard et al., 2011; Temmerman et al., 2013). From a methodological standpoint, rigorous statistical analysis of erosion patterns that integrates geotechnical measurements with hydro-climatic and land-use drivers is essential for designing robust climate adaptation in coastal zones. This study responds to

that need by proposing a geological-survey–based, quantitative, cross-sectional, multi-case analysis that links measurable soil and geomorphic properties to observed erosion metrics and stakeholder perceptions, thereby generating transferable evidence for coastal management across diverse settings.

Globally, sea-level rise and changing extremes frame the risk context in which local geotechnical properties play out. A landmark synthesis highlighted the multiple pathways through which sea-level rise magnifies hazard, including higher base water levels, more frequent thresholds for flooding and wave impact, wetland submergence, and salinization (Nicholls & Cazenave, 2010). Probabilistic projections of extreme sea levels incorporating storms and waves show heterogeneous regional changes but an overarching increase in the frequency of historically rare events, underscoring the potential for accelerated shoreline retreat and damage in exposed settings (Muis et al., 2018). Global assessments estimate substantial increases in coastal flood damages without adaptation and large but often cost-effective adaptation outlays via protection, accommodation, or retreat strategies (Muis et al., 2018). For sandy coasts specifically, recent analyses report that a substantial fraction is already eroding and that many shorelines are likely to retreat further under high-emissions scenarios absent sediment management and protective measures (Vousdoukas et al., 2020). These global perspectives motivate site-specific, data-rich case studies that quantify how much of the observed erosion is statistically attributable to wave climate, storm surge, and rainfall intensity versus geotechnical susceptibility and land-use changes. They also legitimize attention to "green-gray" portfolios, where vegetation-enhanced dunes, marsh restorations, or reef structures attenuate waves and stabilize sediments, potentially lowering life-cycle costs and failure risks compared to exclusively hard defenses. For research design, this international context justifies multi-site comparisons across geomorphic settings and management regimes, enabling cross-sectional identification of consistent drivers and moderators of erosion outcomes.

Empirically, several driver classes recur across the literature. First, wave climate including significant wave height and direction controls the magnitude and gradients of littoral transport, with trends toward higher extremes reported in some ocean basins; ENSO and other teleconnections further modulate interannual coastal responses (Ranasinghe, 2016). Second, rainfall erosivity has increased in many regions, with high-frequency intensity bursts exerting disproportionate geomorphic effects on surface sealing, rilling, and dune or bluff instability (Stevenson et al., 2019). Third, soil mechanical properties especially lower median grain size (D50), lower cohesion, and lower shear strength tend to increase susceptibility to detachment under given hydraulic stresses; geotechnical reviews consolidate these relations and advocate estimating soil resistance from measurable properties rather than treating it as a calibration fudge factor (Kinnell, 2010; Knapen et al., 2007). Fourth, vegetation acts both as a protective cover and as a below-ground reinforcement that increases soil resistance; in coastal settings, marshes and mangroves attenuate waves and facilitate sediment deposition, while vegetated dunes trap aeolian sand and promote berm and foredune stabilization (Ruggiero et al., 2010; Shepard et al., 2011). These mechanisms justify modeling strategies that include (a) additive effects of forcing (waves, surge, rainfall) and susceptibility (geotechnical metrics) and (b) interaction terms capturing moderation by vegetation cover or engineered defenses. They also support site fixed effects to absorb unobserved heterogeneity and robustness checks such as alternative functional forms (e.g., GLMs for positive, skewed erosion rates), penalized regression for collinearity, and spatial regression when residuals exhibit significant autocorrelation.

This study adds to the coastal hazards literature by centering geotechnical soil properties within a statistical modeling framework calibrated by geological survey protocols and enriched by remote sensing and stakeholder data. While global syntheses have clarified the scale of future risk and highlighted the potential of nature-based defenses, there remains a need for case-resolved, cross-sectional evidence that quantifies how much variance in erosion is explained by measurable soil and geomorphic properties versus hydro-climatic forcing and land-use factors. By specifying outcome variables (e.g., shoreline retreat rate, volumetric soil loss) and predictors spanning geotechnical

American Journal of Interdisciplinary Studies
Volume 03, Issue 03 (2022)
Page No: 36 – 67
eISSN: 3067-0470
DOI: 10.63125/xytn3e23

(D50, cohesion, shear strength), geomorphic (slope, elevation), hydro-climatic (rainfall intensity, significant wave height, surge), and land-cover (vegetation %, engineered defenses) domains, and then employing correlation analysis followed by regression with interaction terms (e.g., Wave × Vegetation), the analysis will identify statistically significant drivers and moderators of erosion. The adoption of UAV-enabled SfM, satellite-derived shorelines, and probabilistic extreme sea-level datasets ensures that measured patterns are captured with sufficient spatial resolution and physical realism. Finally, integrating Likert-scale perception data aligns the physical diagnosis with social readiness, providing coastal managers with evidence that is both technically grounded and decision-oriented. As a result, the study contributes: (a) a reproducible, geological-survey–based protocol for data collection; (b) a transparent statistical pipeline with diagnostics and robustness checks; and (c) comparative insights across multiple coastal cases that inform selection and targeting of adaptation measures, including nature-based options where interactions indicate the greatest leverage.

LITERATURE REVIEW

The literature on coastal soil loss and erosion spans interconnected strands that together explain why some shorelines retreat rapidly while others remain comparatively stable under similar climatic forcing. Foundational geomorphology delineates the process regime wave climate, storm surge, tidal range, and rainfall intensity through which energy is delivered to the coast, while geotechnical research specifies how soils of differing texture, plasticity, bulk density, and cohesion resist detachment and transport. Advances in measurement and monitoring have transformed what can be observed: geological surveys now couple stratified field sampling, in-situ strength testing, and laboratory characterization with geospatial products derived from satellite imagery, UAV photogrammetry, and high-resolution digital elevation models. This toolbox enables consistent quantification of shoreline positions, dune and scarp morphodynamics, and volumetric changes over analysis windows short enough to be policy-relevant yet robust to seasonal variability. Parallel developments in hydro-meteorological reanalysis provide standardized covariates significant wave height, storm surge probabilities, rainfall intensity metrics that can be fused with site geotechnics and land-cover information to probe causal structure. On the modeling side, the literature has moved from descriptive case narratives toward multivariate frameworks that relate observed erosion to both external forcing and internal susceptibility, increasingly incorporating interactions to capture moderation by vegetation or engineered defenses. At basin and global scales, comparative assessments establish the context of rising sea level and shifting extremes, but they also underscore the heterogeneity that demands case-resolved evidence grounded in local soils and morphologies. Across social-ecological research, risk perception and institutional capacity emerge as pivotal determinants of which adaptation options are feasible, durable, and cost-effective, motivating the integration of stakeholder surveys alongside physical measurements. What remains comparatively thin and thus motivates the present study is a coherent, reproducible pipeline that starts with geological-survey protocols, harmonizes multi-source geospatial and hydro-climatic data, and then applies a staged statistical analysis (descriptives, correlation, regression with diagnostics and robustness checks) to identify significant drivers and moderators of erosion across multiple sites. Positioning the review around these strands process drivers, geotechnical controls, measurement approaches, and statistical modeling creates a scaffold for evaluating evidence quality, surfacing gaps, and justifying the study's variables, design choices, and hypotheses.

Coastal Erosion Processes and Drivers

Coastal erosion reflects the interplay between external process regimes that supply energy to the shoreline and internal properties that determine how coastlines transform that energy into morphological change. On energetic coasts, storm-wave climate and surge set the dominant timescales and magnitudes of sediment mobilization; shifts in storm sequencing and directional wave power alter alongshore transport gradients, reconfigure embayments, and redistribute erosional "hot spots." A seminal modeling study demonstrated that even without mean sea-level change, reorganizations of storm tracks and wave approach angles can substantially reshape

American Journal of Interdisciplinary Studies
Volume 03, Issue 03 (2022)
Page No: 36 – 67
eISSN: 3067-0470
DOI: 10.63125/xytn3e23

planform coastlines by modulating gradients in alongshore sediment flux accelerating retreat in some segments while promoting accretion in others (Slott et al., 2006). Episodic clusters of extreme wave events provide clear, measurable expressions of these dynamics: during the 2013/2014 North Atlantic winter, an exceptionally energetic wave season coincided with widespread beach and dune erosion along the Atlantic coasts of Europe, revealing how storm-wave forcing propagates into cross-shore sediment losses and coastline rotation within embayed settings (Masselink et al., 2016). Such episodes underscore the primacy of wave climate as a driver of near-term shoreline response and highlight the sensitivity of morphodynamics to variations in storm intensity and directionality. In parallel, high-resolution observations of cliffed coasts show that marine attack at the cliff base, mediated by wave run-up and impact, drives many of the largest discrete retreat events, while the overall retreat statistics display heavy-tailed distributions dominated by a minority of failures (A. P. Young et al., 2011). Together, these strands of evidence frame erosion as an energy-partitioning problem in which wave climate and surge regulate the frequency and magnitude of threshold exceedance at the shoreface and toe, thereby governing both incremental profile change and sudden failures.

Figure 2: Coastal erosion processes and drivers.

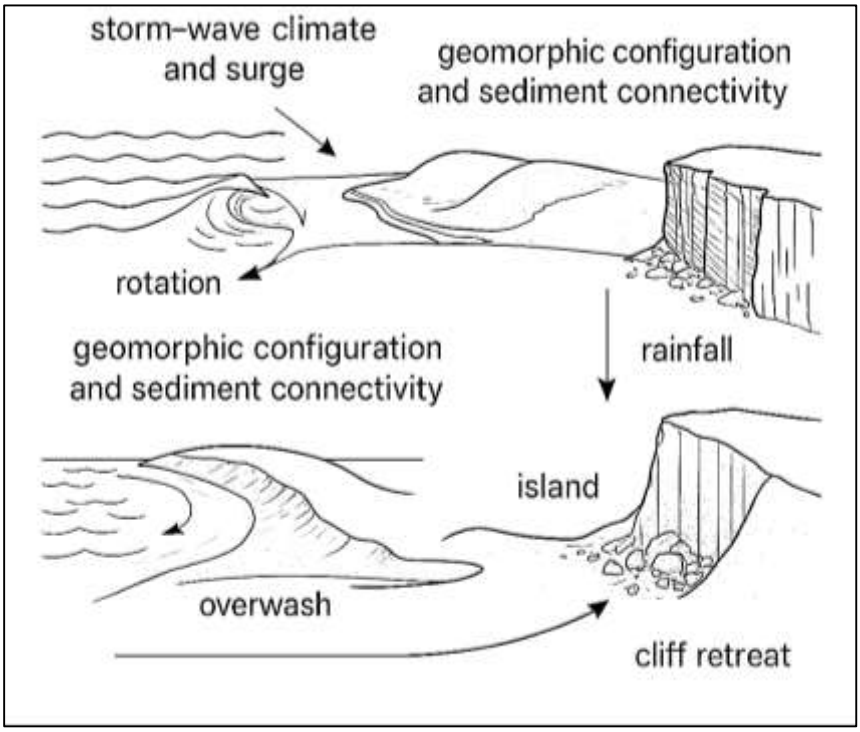

The coastal response to energetic forcing is filtered by geomorphic configuration and sediment connectivity, so that the same offshore conditions can yield divergent morphologies across short distances. Barrier islands and dune-backed beaches exemplify this sensitivity: their storm-scale response depends on the relative elevation of the total water level to dune crest and toe, the alongshore continuity of dune ridges, and the capacity for aeolian and swash processes to rebuild volumes between events. Empirical work on post-storm evolution shows that the rate and extent of dune and beach recovery critically determine subsequent vulnerability where recovery is limited or spatially uneven, barrier segments remain predisposed to enhanced erosion in the next high-water season (Houser et al., 2015). At the scale of embayments and regional coasts, the sign and magnitude of shoreline change are also contingent on longshore sediment budgets: when wave climate imposes persistent transport divergence and sources do not compensate, profiles steepen and retreat accelerates (Danish & Zafor, 2022); conversely, flux convergence can stabilize or rotate beaches without net volumetric loss. Hindcast-based analyses of longshore fluxes along exposed sandy

American Journal of Interdisciplinary Studies
Volume 03, Issue 03 (2022)
Page No: 36 – 67
eISSN: 3067-0470
DOI: 10.63125/xytn3e23

coasts demonstrate substantial spatiotemporal variability in transport direction and magnitude linked to atmospheric circulation regimes, clarifying why erosion and accretion often exhibit coherent but alternating patterns alongshore (Idier et al., 2013). These findings emphasize two practical points for geotechnical-statistical studies: first, that predictor sets must encode not just wave energy but also directional and sequencing information that controls alongshore gradients; and second, that site effects (e.g., headlands, inlets, engineered structures) should be treated as structural modifiers of sediment pathways rather than mere nuisance terms. Ultimately, the dominant cross- and alongshore process couplings run-up exceedance at dunes, collision and overwash potential, and flux divergence explain much of the observed heterogeneity in erosion outcomes across beaches with similar offshore climates.

Cliffed and mixed-sediment coasts illustrate another pathway through which process drivers express themselves, namely via discrete failures that punctuate longer quiescent intervals. Lidar-resolved monitoring reveals that the majority of time steps show no measurable cliff-edge motion; when failures do occur, they tend to cluster temporally and spatially, with marine attack at the base setting primary controls and rainfall acting as a complementary driver of material weakening and pore-pressure changes (Idier et al., 2013; Young et al., 2011). Superimposed on these local triggers are basin- to synoptic-scale patterns in storminess that synchronize forcing across hundreds of kilometers, as captured during the 2013/2014 winter sequence: in addition to the cross-shore sand losses at open-coast beaches, sheltered or partially enclosed sites exhibited beach rotation governed by changes in wave directionality, attesting to the coherence of shoreline response across morphodynamic settings under a common atmospheric regime (Houser et al., 2015; Masselink et al., 2016). Finally, theoretical and numerical work on storm-pattern change highlights that coastlines are not passive "tapes," but dynamic systems that can reorganize dramatically when the directional statistics of waves shift even absent large changes in mean conditions because alongshore sediment transport is a nonlinear function of wave approach angle (Slott et al., 2006). For a quantitative, geological-survey–anchored research design, these insights motivate (a) explicit cross- and alongshore metrics of exposure; (b) outcome definitions that separate incremental profile change from discrete failures; and (c) model specifications that allow interactions between forcing and geomorphic context (e.g., ridge continuity, cliff lithology) to emerge statistically. In sum, coastal erosion patterns arise from the coupling of event-scale hydrodynamics with sediment-budget constraints and morphological thresholds, which together produce the observed mosaics of retreat, stability, and rotation across neighboring segments.

Geotechnical Controls on Soil Loss and Erosion

Geotechnical properties govern how coastal soils detach, transport, and reorganize under hydrodynamic forcing, and they do so through a small set of measurable parameters that directly influence detachment thresholds and rates. At the grain scale, particle size distribution and fabric regulate frictional resistance, while electrochemical bonding among clay minerals imparts cohesion (Rezaul, 2021); together these shape the critical shear stress (τ_c) a soil can withstand before erosion begins and the erodibility coefficient (k_d) that modulates subsequent detachment rates. In cohesive and mixed (sand–clay) shorelines, microstructure, organic content, and consolidation state alter pore-scale strength and hence macroscopic erodibility; even modest shifts in plasticity index or water content can move a soil from a friction-dominated to a cohesion-dominated response (Grabowski et al., 2011). This helps explain why apparently similar intertidal or back-barrier surfaces show order-of-magnitude differences in erodibility during the same storm. A comprehensive synthesis across riverine and coastal settings concluded that cohesion (via clay mineralogy and salinity), consolidation, and biological binding/bioturbation jointly set τ_c and erosion rate more than hydraulics alone an insight that underpins modern excess-shear and mechanistic detachment formulations used in coastal risk models (e.g., beachface lowering or marsh-edge retreat modules) (Grabowski et al., 2011). These reviews emphasize that prediction improves when geotechnical descriptors (plasticity, bulk density, undrained shear strength) are explicitly integrated rather than

American Journal of Interdisciplinary Studies
Volume 03, Issue 03 (2022)
Page No: 36 – 67
eISSN: 3067-0470
DOI: 10.63125/xytn3e23

inferred from texture alone, because cohesive matrices often display threshold-like behavior not captured by grain-size metrics.

Figure 3: Geotechnical controls on soil loss and erosion

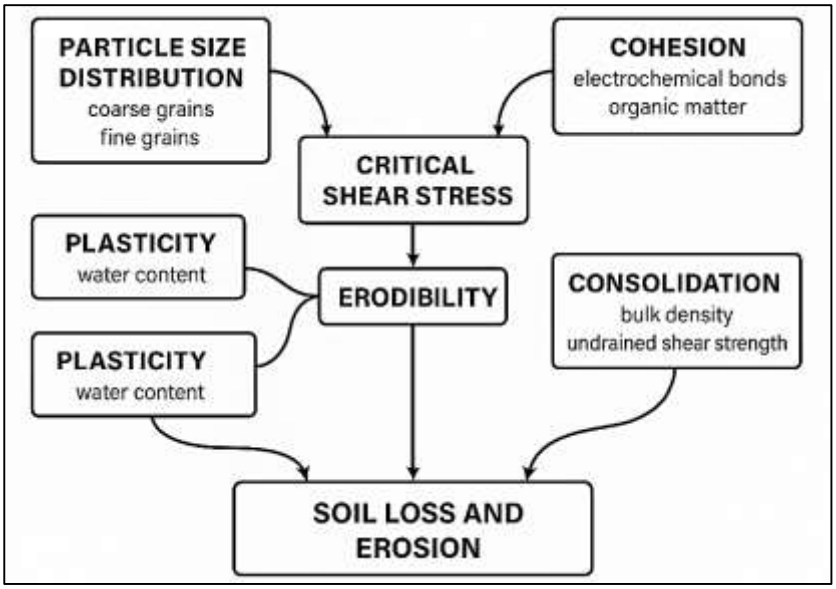

Turning to measurement, the submerged Jet Erosion Test (JET) has become the standard in situ tool for estimating τ_c and k_d of cohesive banks, marsh edges, and embankments, and it has been increasingly applied in coastal case studies to parameterize detachment under wave-current forcing. Methodological work shows that the way JET data are reduced (Blaisdell/iterative/scour-depth solutions) can bias τ_c upward or downward and change k_d by factors of two or more because of jet confinement and bed roughness effects; hence, protocols and model choice materially affect any regression-based erosion forecast built on those parameters (Clark & Wynn, 2007; Karamigolbaghi et al., 2017). These findings matter in coastal adaptation designs where small changes in τ_c cascade into large differences in predicted retreat or scour depth under design storms. The same assessments recommend standardized reporting (soil water content, bulk density, plasticity, salinity) and multiple tests per layer to capture vertical variability especially important in stratified shorefaces and marsh scarps where a thin clayey cap overlies sandier substrates. For quantitative studies like the present multi–case survey, adopting a consistent JET reduction method and documenting sample state (remolded vs. intact, degree of consolidation) improves comparability across sites and supports hierarchical modeling of k_d and τ_c as functions of plasticity index, fines content, and undrained shear strength (Clark & Wynn, 2007; Karamigolbaghi et al., 2017).

A final dimension is spatial variability across sites and scales: even within one estuary or back-barrier reach, τ_c and k_d often vary by one to several orders of magnitude because of layering, moisture regimes, vegetation rooting, and antecedent wetting–drying histories (Danish & Kamrul, 2022). Watershed- and reach-scale syntheses using dozens to hundreds of JETs show that erodibility parameters can cluster by lithostratigraphic unit but still drift alongshore with sediment delivery and vegetative stabilization; critically, models calibrated with single "representative" parameter sets underperform when lateral variability is high (Daly et al., 2015; Jahid, 2022). For coastal applications, this implies that the case-selection and sampling strategy should stratify by geomorphic unit (e.g., dune toe, back-barrier marsh edge, tidal creek bank) and by soil state (bulk density/moisture), and that regression models should allow random effects or site-level intercepts when relating τ_c and k_d to predictors such as plasticity index, median grain size (D50), and vane shear strength. Studies that compared mechanistic (Wilson-type) formulations with classical excess-shear models found that, while both can be made to fit, mechanistic models sometimes better accommodate cohesive

behavior in mixed sediments; still, both require robust, site-specific geotechnical inputs to avoid biased retreat predictions (Ismail, 2022). For this project's quantitative, cross-sectional, multi–case design, incorporating geotechnical covariates (plasticity, water content, bulk density, shear strength) into the statistical analysis plan and collecting sufficient replicates per layer and site will reduce parameter uncertainty and increase the explanatory power of correlations and regressions linking soil properties to observed erosion metrics (Enlow et al., 2017).

Measurement and Monitoring Approaches

Reliable measurement of coastal soil loss and shoreline change begins with agreeing on what exactly is being measured i.e., which shoreline indicator and then applying methods that detect that indicator consistently through time and across sites. A seminal review formalized this two-step logic ("define, then detect") and cataloged common shoreline proxies (e.g., high-water line, vegetation line, instantaneous waterline, dune toe) alongside their biases under varying wave, tide, and light conditions; critically (Hossen & Atiqur, 2022), it showed that indicator choice can shift reported erosion rates by both sign and magnitude, and recommended documenting the indicator, tidal stage, and illumination for every mapped shoreline (Boak & Turner, 2005; Kamrul & Omar, 2022). In field-centric geological surveys, this implies building transect datasheets around unambiguous features (e.g., scarp toe, dune crest) and pairing GNSS profiles with notes on runup and moisture so the same indicator is re-located in follow-on campaigns. Where frequent mapping is needed, coastal video monitoring systems (e.g., Argus) have proven adept at producing "time-exposure" images from rapid-sampled frames that smooth swash and reveal quasi-instantaneous shoreline position; long, rectified image sequences enable estimation of intertidal width, wave runup statistics, and seasonal beach rotation at daily-to-weekly cadence, with careful calibration to ground control (Holman & Stanley, 2007; Razia, 2022). Together, these strands underscore a principle essential to multi–case, cross-sectional designs: measurement is not only about spatial accuracy; it is about protocol reproducibility, so that apparent differences between sites reflect process, not method.

Advances in satellite and airborne remote sensing have transformed coastal monitoring from episodic snapshots to scalable, comparable time series. On the optical side, sub-pixel shoreline algorithms for Landsat-class imagery register multitemporal scenes precisely and infer the waterline with uncertainties on the order of a pixel or better, enabling decadal-to-multidecadal shoreline reconstructions at hundreds to thousands of kilometers of coast with transparent error budgets (Pardo-Pascual et al., 2012; Sadia, 2022). Global applications leveraging the full Landsat archive demonstrate how, once geometric registration and waterline extraction are standardized, one can compile continental assessments of sandy shoreline change, detect erosion and accretion mosaics, and evaluate management and sediment-budget hypotheses against consistent evidence (Luijendijk et al., 2018). For geological-survey–based studies, these products are powerful covariates and baselines: satellite-derived trends can (a) guide where to place high-resolution transects and UAV photogrammetry; (b) benchmark field-measured retreat against long-term tendencies; and (c) expose directional asymmetries (e.g., rotation) that might otherwise be missed by sparse transects. Importantly, the remote sensing pipeline is only as reliable as its tide and wave context; thus, field campaigns should log tidal stage and wave conditions to align in-situ indicators with the tide-filtered, time-averaged waterline seen from space. In practice, robust integration looks like this: define the indicator (e.g., vegetation line for dunes, wet-dry line for sandy beaches), use sub-pixel extraction for historical context, and then complement it with GNSS/UAV surveys that resolve cross-shore profiles and scarp geometry at centimeter-to-decimeter scales on the analysis date (Boak & Turner, 2005; Holman & Stanley, 2007).

American Journal of Interdisciplinary Studies
Volume 03, Issue 03 (2022)
Page No: 36 – 67
eISSN: 3067-0470
DOI: 10.63125/xytn3e23

Figure 4: Measurement and monitoring approaches for coastal soil loss

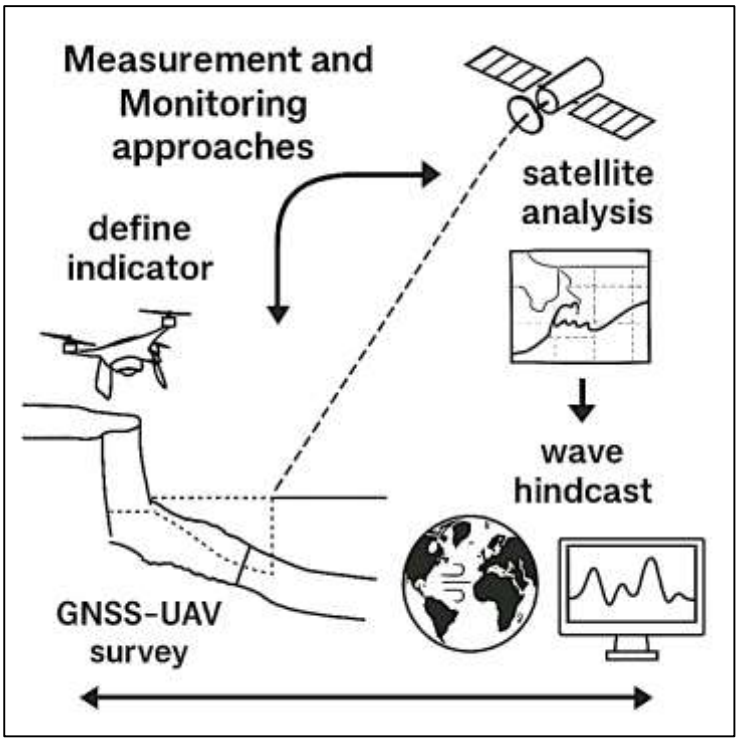

Hydro-meteorological forcing datasets are the third pillar: without consistent wave, wind, and rainfall drivers, it is difficult to attribute measured morphological change to process. Modern global reanalyses now deliver hourly-to-subdaily time series of winds, pressure, waves, and precipitation on uniform grids back to the 1970s–1950s, supporting both event attribution and long-term climatologies; among these, ERA5 substantially improves temporal resolution and physical realism relative to its predecessors and has become a standard backbone for coastal forcing reconstructions and extreme-water-level modeling (Hersbach et al., 2020). In a measurement-and-monitoring context, ERA5 (and wave reanalyses derived from it) can be mined for storm sequencing, fetch-aligned wind vectors, and significant wave height time series that explain when and why transect-scale erosion spikes occur. The craft lies in fusing scales: use ERA5 to define storm windows and directional wave climates; match those windows to video-derived runup proxies and satellite waterlines; and anchor interpretation with geological survey transects and cores that document the geotechnical state (moisture, density, plasticity, shear strength) of eroding faces. In analysis, this fusion supports outcome definitions that separate gradual profile change from threshold-driven failures, and predictor sets that include not only the magnitude of forcing but its directionality and sequencing. Method sections should therefore specify: indicator definitions; image sources and sub-pixel extraction settings; ground-control procedures; tide/wave harmonization; and the reanalysis products (resolution, variables, post-processing) used to derive event and climatological covariates. This ensures that reported erosion rates and soil-loss indices are traceable, comparable, and explainable across cases qualities that are indispensable for robust statistical modeling and credible climate adaptation evidence (Hersbach et al., 2020; Pardo-Pascual et al., 2012).

American Journal of Interdisciplinary Studies
Volume 03, Issue 03 (2022)
Page No: 36 – 67
eISSN: 3067-0470
DOI: 10.63125/xytn3e23

Statistical and Predictive Modeling in Coastal Erosion

Predictive modeling of coastal erosion has evolved from site-specific heuristics to formal statistical and hybrid process–statistical frameworks that quantify uncertainty and accommodate heterogeneous drivers. A foundational step is to represent how hydrodynamic forcing translates into shoreline impact metrics that are suitable as predictors or as mechanistic submodels within a statistical pipeline. Empirical parameterizations of wave setup, swash, and total runup provide precisely this bridge by expressing exceedance levels as compact functions of offshore wave height, period, and beach slope; these relations are widely used to estimate collision and overwash regimes and to generate event-scale exposure variables for regression and risk modeling (Stockdon et al., 2006). Once exposure metrics are defined, descriptive statistics and correlation analysis establish first-order associations and multicollinearity structure among candidate predictors (e.g., runup exceedance frequency, storm sequencing, antecedent morphology, vegetation cover, geotechnical indices). Multiple regression ordinary least squares or generalized linear models for positive, skewed outcomes then provides effect-size estimates, while penalized variants (ridge/lasso) address high dimensionality. Crucially, modelers must incorporate diagnostics for heteroskedasticity, influence, and spatial autocorrelation; when residuals remain spatially structured after covariate control, spatial lag or error models are warranted. Event-based formulations benefit from interaction terms capturing moderation (e.g., runup × vegetation or storm cluster × antecedent beach state), and cross-sectional multi-case designs often improve comparability through site fixed effects. These statistical elements create a reproducible scaffold into which process-derived predictors such as parameterized runup, surge heights, and longshore transport proxies can be embedded, combining physical intelligibility with inferential transparency and uncertainty quantification at the scales relevant to management (Gutierrez et al., 2011; Stockdon et al., 2006).

Figure 5: Statistical and predictive modeling in coastal erosion

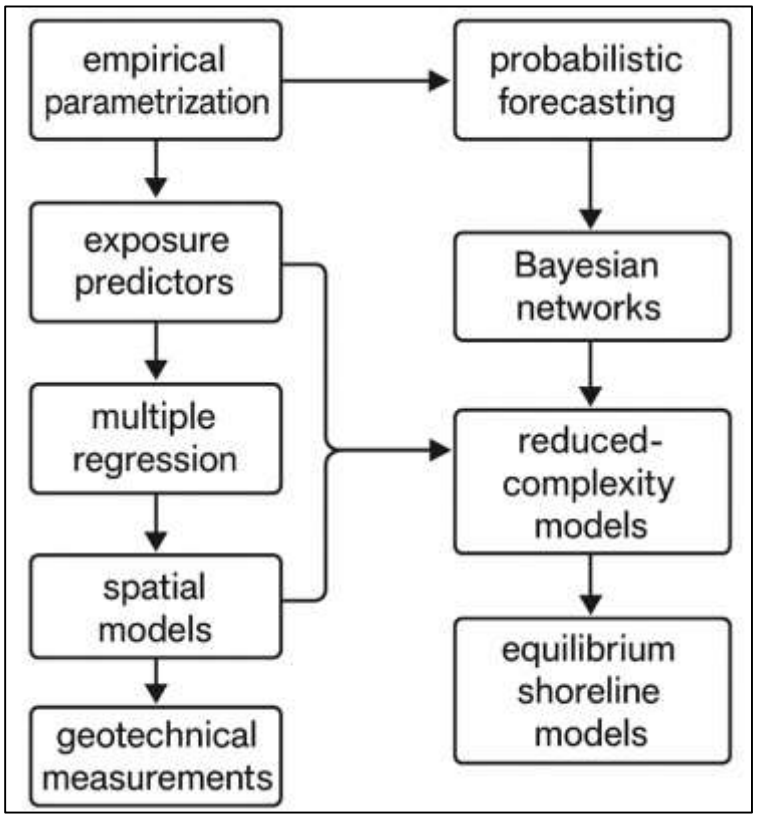

American Journal of Interdisciplinary Studies
Volume 03, Issue 03 (2022)
Page No: 36 – 67
eISSN: 3067-0470
DOI: 10.63125/xytn3e23

Complementing probabilistic methods are reduced-complexity dynamical models that encode dominant feedbacks between wave climate and shoreline position in compact equations amenable to statistical estimation and hindcast–forecast use. Generalized equilibrium shoreline models posit that beaches fluctuate around a wave-climate–dependent equilibrium, with departures relaxing toward that equilibrium at rates set by local morphology and sediment supply; when calibrated, such models skillfully reproduce interannual shoreline variability across diverse coasts and offer parsimonious predictors for future states under altered forcing (Splinter et al., 2014). Recent advances have extended these ideas by coupling cross-shore and longshore components and embedding sea-level rise trajectories to simulate multi-decadal evolution under changing storm regimes, producing ensemble forecasts that account for both climate forcing and internal morphodynamic memory (Vitousek et al., 2017). These streamlined dynamical formulations are particularly powerful when integrated with statistical layers: equilibrium parameters can be estimated via regression against long records of wave, water level, and shoreline position; hierarchical structures allow site-level random effects to capture unobserved controls; and data-assimilation steps can periodically re-initialize forecasts with the latest satellite- or UAV-derived shorelines. For geological-survey–based studies, which add geotechnical covariates (e.g., cohesion, D50, undrained shear strength), reduced-complexity models can be augmented with terms that scale response rates or thresholds according to measured substrate resistance, thereby linking physical soil properties to emergent shoreline dynamics in a statistically tractable way. The result is a coherent predictive toolkit: empirical runup parameterizations to build exposure predictors; probabilistic or Bayesian-network frameworks to quantify event-scale risks; and equilibrium-type shoreline models to forecast trajectory envelopes each calibrated and validated with reproducible statistical procedures and fused, where appropriate, with geotechnical measurements to capture susceptibility.

METHOD

This study has adopted a geological-survey–based, quantitative, cross-sectional, multi-case design to examine geotechnical soil loss and coastal erosion patterns under contemporary hydro-climatic forcing. We have structured the methodology to ensure comparability across cases while preserving site-specific detail essential to geotechnical interpretation. Case locations have been selected using explicit inclusion criteria (documented active erosion, accessible shore-parallel infrastructure, availability of hydro-meteorological records) and exclusion criteria (fully armored shorelines where natural processes have been masked, or sites lacking permissions), and have been stratified by geomorphic setting (open sandy beach, dune-backed barrier, marsh edge or scarped bluff). Within each case, shore-perpendicular transects have been established and have provided the spatial framework for synchronized field sampling, topographic profiling, and stakeholder surveying. Geological survey protocols have specified standardized collection of soils (0–30 cm surface and deeper cores as applicable), in-situ measurements (moisture, vane shear or penetrometer resistance), and high-precision GNSS positioning, while laboratory analyses have produced particle size distributions (including D10/D50), Atterberg limits, bulk density, and undrained/direct-shear strength. To capture morphological context, we have compiled GIS/RS datasets (satellite-derived shorelines, orthomosaics, and where available UAV-SfM elevation products) and have co-registered them to the transect network. Hydro-climatic drivers have been assembled from quality-controlled wave, tide, rainfall, and storm-surge records and have been temporally aligned to the field campaign window to derive exposure metrics (e.g., significant wave height statistics, runup proxies, rainfall intensity indices). A parallel Likert five-point survey has been administered to capture perceived risk, experienced impacts, and willingness to adopt adaptation measures in communities proximate to each transect. Data management has followed a pre-specified codebook and chain-of-custody procedures, and QA/QC checks (duplicates, instrument calibrations, range and logic screens) have been documented. The analysis plan has proceeded in a staged manner: (i) data auditing and preprocessing (missingness assessment, transformation and standardization), (ii) descriptive statistics and mapped summaries, (iii) bivariate correlation screening, and (iv) multivariable

American Journal of Interdisciplinary Studies
Volume 03, Issue 03 (2022)
Page No: 36 – 67
eISSN: 3067-0470
DOI: 10.63125/xytn3e23

modeling that has incorporated diagnostics for multicollinearity, heteroskedasticity, influence, and spatial autocorrelation. Primary regressions have pooled observations with site fixed effects and have tested theoretically motivated interactions (e.g., wave energy × vegetation cover). Power calculations and sampling targets have been specified a priori to ensure statistical adequacy, and all steps have been scripted for reproducibility.

Figure 6: Methodoly of this research.

American Journal of Interdisciplinary Studies
Volume 03, Issue 03 (2022)
Page No: 36 – 67
eISSN: 3067-0470
DOI: 10.63125/xytn3e23

Research Design

This study has employed a geological-survey–based, quantitative, cross-sectional, multi–case research design to identify and explain spatial patterns of coastal soil loss and shoreline erosion across contrasting geomorphic settings. We have purposively selected multiple coastal cases using transparent inclusion criteria (recent documented erosion, access for shore-perpendicular transects, availability of wave–tide–rainfall records, and management relevance) and exclusion criteria (fully armored segments that mask natural processes unless treated as a separate stratum). Within each case, we have established transects at 200–500 m spacing and drawn stratified random sampling points across key units (beachface, dune toe/crest, marsh edge, scarp toe) to collect soils and geotechnical measurements. Geological survey protocols have specified standardized in-situ observations (moisture, vane shear or penetrometer resistance), GNSS waypointing of morphological indicators (e.g., wet-dry line, vegetation line, dune/scarp reference points), and chain-of-custody procedures for laboratory testing of particle size distribution (including D10/D50), Atterberg limits, bulk density, and undrained/direct-shear strength. To situate these measurements, we have compiled co-registered GIS/remote-sensing layers (historical shoreline proxies, land cover, and where available UAV-SfM orthomosaics/DEMs) and aligned hydro-climatic drivers (significant wave height/period, tidal range, surge metrics, rainfall intensity) to the field window to derive exposure indicators and storm sequencing variables. A parallel Likert five-point survey has captured perceived risk, experienced impacts, and willingness to adopt adaptation measures among residents and practitioners proximate to transects. Data management has followed a master schema linking samples, tests, transects, and respondents, with QA/QC via duplicates, calibration logs, range and logic checks, and spatial topology validation. The analysis plan has proceeded from preprocessing and descriptives to correlation screening and multivariable modeling that includes site fixed effects and theory-driven interactions (e.g., Wave × Vegetation), with diagnostics for multicollinearity, heteroskedasticity, influence, and spatial autocorrelation and robustness via GLM, penalized, and spatial alternatives. Ethics protocols (informed consent, anonymization, secure storage) and safety/permit compliance have been maintained throughout.

Cases, Sampling, and Setting

The study has delineated multiple coastal cases that have exhibited active erosion within the past three to five years and have provided reliable hydro-meteorological records, access, and management relevance. Each case has been stratified by geomorphic setting (open sandy beach, dune-backed barrier, marsh edge, or scarped bluff), and alongshore analysis units (~0.5–2.0 km) have been established to standardize observation scales. Within each unit, shore-perpendicular transects at 200–500 m spacing have been installed, and stratified random sampling points across key sub-environments (beachface, dune toe/crest, marsh edge, scarp toe) have been drawn to capture geotechnical and morphological variability. Inclusion criteria have required (a) documented shoreline change detectable over a recent interval, (b) safe and legal site access, (c) proximity to wave, tide, and rainfall gauges or defensible reanalysis substitutes, and (d) community presence suitable for administering the parallel stakeholder survey. Exclusion criteria have removed fully armored or dredge-dominated segments that have masked natural processes, parcels without permissions, and locations where safety constraints have persisted. For each selected point, field teams have collected soils (0–30 cm and deeper cores where applicable), have recorded in-situ moisture and vane-shear or penetrometer resistance, and have logged GNSS positions for morphological indicators to ensure geospatial repeatability. To ensure statistical adequacy, a priori power analysis for multiple regression has informed the minimum number of observations per predictor, and planned sampling totals have been inflated by ~15% to offset attrition and unusable specimens. Community respondents proximate to transects have been recruited via stratified quotas (settlement/occupation), and informed consent procedures have been completed prior to interviews. Permissions and safety plans have been filed with local authorities, and a chain-of-custody protocol has been enforced for all samples. This sampling frame has balanced cross-case

American Journal of Interdisciplinary Studies
Volume 03, Issue 03 (2022)
Page No: 36 – 67
eISSN: 3067-0470
DOI: 10.63125/xytn3e23

comparability with site-specific resolution, and it has provided a defensible basis for pooling data with site fixed effects while preserving heterogeneity essential to geotechnical interpretation.

Variables and Measures

The study has operationalized a structured set of outcomes, predictors, controls, and survey constructs to ensure comparability across cases and traceability from field to analysis. The primary outcomes have comprised (Y1) an erosion rate ($m \cdot yr^{-1}$ equivalent) that has been derived from standardized shoreline-position change over the most recent defendable interval and re-referenced to the cross-sectional study window, and (Y2) a soil-loss index ($t \cdot ha^{-1}$ proxy) that has been computed from plot-scale volumetrics or DEM-of-Difference where available and otherwise from calibrated transect geometry and profile change. Each outcome has been paired with an explicit shoreline or scarp indicator (e.g., wet–dry line, vegetation line, dune toe, scarp toe), which field teams have documented at acquisition and which GIS processing has carried through as metadata. Geotechnical predictors have included particle-size metrics (D10, D50, sorting), Atterberg limits (LL, PL, PI), bulk density, near-surface gravimetric water content, and undrained/direct-shear strength; these have been measured under a documented sample state (intact/remolded), and units and methods have been encoded in a shared codebook. Geomorphic predictors have encompassed beach/dune slope, elevation, curvature, presence of dunes/wetlands, and distance to inlets/headlands, which GNSS profiles and orthomosaics have supplied. Hydro-climatic predictors have consisted of significant wave height/period summaries, tide and surge statistics, runup/total water-level proxies aligned to the campaign window, and rainfall intensity indices; directional and sequencing metrics (e.g., storm clusters) have been derived to capture exposure asymmetry. Human/land-cover variables have included vegetation cover (%), impervious fraction, presence/length of hard defenses, and dredging/mining indicators. Survey constructs have captured perceived erosion risk, experienced impacts, trust in measures, and willingness to adopt adaptation (Likert 1–5); item wording, scales, and skip logic have been pretested, and composite indices have been specified a priori. Controls have included site fixed effects and an exposure/fetch index. All variables have undergone unit harmonization, range and logic checks, documented transformations (e.g., log for skew), and z-standardization for modeling; missingness patterns have been audited, and imputation rules have been recorded for MAR/MCAR cases.

Data Sources and Collection

The study has assembled and collected data through four coordinated streams geological survey, laboratory testing, geospatial/remote sensing, and hydro-meteorological forcing supplemented by a parallel stakeholder survey, all synchronized to the cross-sectional field window. Field teams have implemented a standardized geological survey protocol along shore-perpendicular transects: they have logged GNSS baselines, waypoints for morphological indicators (wet–dry line, vegetation line, dune/scarp toe and crest), and photographic quadrats; they have extracted soils at 0–30 cm and, where stratigraphy has warranted, deeper cores using hand augers or piston corers; and they have recorded in-situ moisture and vane-shear or penetrometer resistance together with notes on sediment fabric, vegetation rooting, groundwater, and microtopography. Samples have been labeled with unique IDs, sealed, and refrigerated or air-dried per matrix, and a chain-of-custody ledger has been maintained from field to laboratory. In the laboratory, technicians have processed samples for particle-size distribution (sieve/hydrometer), Atterberg limits (LL, PL, PI), bulk density, and undrained or direct-shear strength, and they have documented instrument calibrations, duplicates (~10%), and blanks; results have been entered into a master codebook with units, methods, and detection notes. The geospatial/RS stream has compiled co-registered historical shorelines, orthomosaics, and, where available, UAV-SfM digital elevation models; scenes have been orthorectified to common projections and vertical references, and transect cross-sections have been extracted to align with field indicators. The hydro-met stream has drawn significant wave height/period, tidal range, surge metrics, and rainfall intensity from nearby gauges or vetted reanalyses; these series have been gap-screened, temporally filtered to the campaign window, and summarized into exposure and storm-sequencing metrics. A structured Likert five-point survey has

American Journal of Interdisciplinary Studies
Volume 03, Issue 03 (2022)
Page No: 36 – 67
eISSN: 3067-0470
DOI: 10.63125/xytn3e23

been administered to residents and practitioners proximate to transects, with pretested items, informed consent, and anonymization; enumerators have logged responses on tablets with built-in validation. All streams have been integrated in a version-controlled repository; data have undergone range and logic checks, timestamp reconciliation, spatial topology validation, and metadata completion so that every observation has remained traceable from raw acquisition to analysis-ready tables.

Statistical Analysis Plan

The analysis has proceeded in staged, reproducible steps that have linked data auditing to inference and robustness. First, we have conducted a comprehensive pre-processing audit: unit harmonization, duplicate detection, cross-field logic checks, and assessment of missingness mechanisms (MCAR/MAR) using indicator models; where appropriate, we have implemented multivariate imputation with passive imputation for derived fields and have flagged imputed cells in the metadata. Continuous variables have been screened for skew and kurtosis, and we have applied monotone transformations (e.g., log, Box-Cox) where diagnostics have indicated; all predictors have then been z-standardized to enable effect-size comparison. Second, we have produced descriptive statistics and cartographic summaries (means, SDs, ranges; transect heat maps) and have generated correlation matrices (Pearson/Spearman as warranted) with variance inflation factors (VIF) to pre-empt multicollinearity; highly collinear predictors have been culled or orthogonalized. Third, we have specified the primary regression as a pooled cross-sectional model with site fixed effects, estimating OLS with heteroskedasticity-consistent (HC3) standard errors; where the outcome has been strictly positive and right-skewed, we have fitted GLMs with Gamma/log link. The modeling set has incorporated theoretically motivated interactions (e.g., Wave × Vegetation; Rainfall × Cohesion). Assumption checks have included linearity (component-plus-residual plots), heteroskedasticity (Breusch–Pagan/White), influence (Cook's D, DFbetas), and residual normality (Q–Q). To address spatial dependence, we have computed Global Moran's I on residuals using contiguity and distance-band weights; where significant, we have estimated spatial lag/error models and compared results. Model selection has relied on AICc/BIC, adjusted R^2, and 5-fold cross-validation (RMSE/MAE); where predictor sets have remained high-dimensional, we have fit ridge/lasso paths to stabilize estimates and inform parsimony. Uncertainty has been characterized with cluster-robust standard errors (by site), nonparametric bootstrap confidence intervals, and leave-one-case-out sensitivity. For Likert survey constructs, we have computed Cronbach's α, performed EFA as needed, formed composite indices, and examined ordinal logistic or linear models linking perceptions to measured hazards. All code and outputs have been version-controlled, and reporting has included coefficient estimates, SEs, 95% CIs, fit metrics, and full diagnostic panels for transparency.

Regression Models

The primary inferential engine has been a pooled cross-sectional regression that has related erosion outcomes to geotechnical, geomorphic, hydro-climatic, and human/land-cover predictors while absorbing unobserved case heterogeneity through site fixed effects. We have specified the baseline as an ordinary least squares (OLS) model for normally distributed outcomes and, when outcomes have been strictly positive and right-skewed, as a generalized linear model (GLM) with Gamma family and log link. In both formulations, all continuous predictors have been z-standardized so that coefficients have represented changes in the outcome per one standard deviation of the predictor, improving comparability across heterogeneous units (e.g., kPa, mm·hr^{-1}, % cover). To minimize omitted-variable bias from persistent, unmeasured site characteristics (e.g., sediment supply peculiarities, governance context), we have included site indicator variables and have employed cluster-robust (HC2/HC3) standard errors at the site level. We have tested linearity assumptions with component-plus-residual plots and have inspected studentized residuals for structure; where curvature has emerged, we have added polynomial terms or monotone transformations that have been pre-registered in the codebook. To address heteroskedasticity, we have estimated heteroskedasticity-consistent covariance matrices and, as a robustness step,

American Journal of Interdisciplinary Studies
Volume 03, Issue 03 (2022)
Page No: 36 – 67
eISSN: 3067-0470
DOI: 10.63125/xytn3e23

weighted least squares using variance functions derived from residual diagnostics. The baseline and GLM specifications used in this study have been summarized in Table 1 with explicit notation, link functions, and error structures, ensuring that model decisions have remained transparent and reproducible across cases. Finally, because outcomes have been measured on common indicators (e.g., dune toe, scarp toe), we have harmonized intercepts by centering outcomes within site where appropriate, which has stabilized estimation without erasing meaningful cross-site contrasts that the fixed effects have already captured.

Table 1. Model specifications and notation

Model	Outcome (Y)	Systematic component	Link / Error	Notes
OLS (Fixed Effects)	Erosion rate (centered/standardized as needed)	$Y_i = \beta_0 + X_i\beta + S_i\gamma + \varepsilon_i$	Identity / $\varepsilon_i \sim$ i.i.d. with HC2/HC3 SEs	S_i are site dummies (fixed effects)
GLM (Gamma)	Positive erosion or soil-loss index	$E(Y_i \cdot) = \exp(\beta_0 + X_i\beta + S_i\gamma)$	Log link / Gamma	Used for right-skewed, positive Y
Moderation (OLS/GLM)	As above	Add $(X_1 \times X_2)$ (e.g., Wave × Vegetation) to X_i	As above	Predictors centered and standardized
Spatial Error / Lag	As above	$Y = X\beta + S\gamma + u$, where $u = \lambda Wu + \xi$ or $Y = \rho WY + X\beta + S\gamma + \varepsilon$	Identity / ML or GMM	W is distance-band weight matrix
Penalized (Ridge/Lasso)	As above	minimize$(\|Y - X\beta\|^2 + \alpha\|\beta\|^2)$ or $(\alpha\|\beta\|_1)$	Identity / CV-tuned α	Used for collinearity and selection
Quantile	As above	minimize $\Sigma_i \rho_\tau(Y_i - X_i\beta)$	Check loss / $\tau \in \{0.5, 0.75, 0.9\}$	Targets median and upper tails

Power and Sample Considerations

The study has implemented a priori and ongoing power procedures to ensure that estimated effects have been statistically detectable under plausible variance and clustering. For the geotechnical–erosion models, we have conducted prospective power analysis for multiple regression (fixed model, R2R^2R2 deviation from zero) with two-sided α=0.05\alpha=0.05α=0.05, desired power ≥0.80\ge 0.80≥0.80, and a medium effect target (f2=0.15f^{2}=0.15f2=0.15) after accounting for site fixed effects and the number of candidate predictors post-screening. Anticipated design effects from within-site clustering have been incorporated via DEFF=1+(m−1)ρDEFF = 1 + (m-1)\rhoDEFF=1+(m−1)ρ, where mmm has represented average observations per site and ρ\rhoρ the intra-class correlation; required sample sizes per model have therefore been multiplied by DEFFDEFFDEFF to preserve nominal power. Because interaction terms (e.g., Wave × Vegetation) have tended to require larger samples, we have computed minimum detectable effects (MDEs) for interactions at observed predictor SDs and have inflated sampling targets accordingly. For the Likert survey, we have applied Cochran's formula with finite population correction where frames have been bounded, and we have stratified quotas by settlement/occupation to control variance; expected response rates and item nonresponse have been folded into targets with a 15–20% attrition buffer. Pilot data (~25–30 respondents per site) have been used to update variance, ICC, and

American Journal of Interdisciplinary Studies
Volume 03, Issue 03 (2022)
Page No: 36 – 67
eISSN: 3067-0470
DOI: 10.63125/xytn3e23

correlation structures, after which we have run sensitivity analyses mapping power over f2∈[0.05,0.25]f^{2}\in[0.05,0.25]f2∈[0.05,0.25] and ρ∈[0.02,0.20]\rho\in[0.02,0.20]ρ∈[0.02,0.20] to assess robustness. Within sites, we have targeted 10–15 analyzable observations per final predictor as a guardrail against overfitting, with additional replicates planned for layers exhibiting high geotechnical variability. The sampling plan has allocated totals proportionally to alongshore analysis units while reserving a minimum floor per unit to stabilize fixed-effect estimation. Throughout fieldwork, realized sample counts, missingness, and leverage diagnostics have been monitored against these thresholds; when shortfalls have emerged, contingency transects or survey waves have been triggered under pre-approved permits so that the final dataset has retained the intended power for primary effects and theoretically motivated interactions.

Reliability and Validity

The study has instituted multi-layered procedures to ensure that measurements and inferences have achieved high reliability and validity across geotechnical, geospatial, hydro-climatic, and survey streams. Instrument reliability has been supported by documented calibration schedules for balances, ovens, hydrometers, sieves, penetrometers, and vane shear devices; laboratories have logged 10% duplicates and periodic blanks, and have reconciled results via pre-specified acceptance bands before release to analysis. Field reliability has been strengthened through standardized operating procedures, inter-observer training, and paired observations on a rotating 10% subsample of transect points; GNSS waypointing and indicator mapping (wet–dry line, vegetation line, dune/scarp references) have been repeated at selected sites to quantify positional repeatability. For the stakeholder survey, the instrument has undergone cognitive pretesting and a pilot, after which internal consistency has been evaluated (Cronbach's α for each multi-item construct), item–total correlations have been screened, and poor items have been revised or retired. Construct validity has been examined through KMO sampling adequacy and Bartlett's test, followed where warranted by exploratory factor analysis with oblique rotation and confirmatory checks on the finalized structure. Measurement validity on the physical side has been enhanced by triangulation among field profiles, laboratory properties, and remote-sensing products (orthomosaics, DEMs, historical shorelines); shoreline indicator definitions have been carried as metadata so that outcomes have remained traceable to consistent features. Internal validity of the statistical models has been addressed by inclusion of site fixed effects to absorb unobserved case heterogeneity, by systematic confounder control, and by comprehensive diagnostics (linearity, multicollinearity via VIF, heteroskedasticity, influence, and Global Moran's I on residuals) with corrective re-estimation using robust, weighted, penalized, or spatial formulations as indicated. Common-method bias in the survey stream has been mitigated procedurally (separated item blocks, neutral wording, anonymity) and assessed analytically (single-factor screen and alternative latent-method specifications). Missing data processes have been audited (MCAR/MAR tests), and imputation has been performed under transparent rules with sensitivity checks against complete-case analyses. External validity has been supported by purposive case diversity, explicit context documentation, and leave-one-case-out tests to evaluate generalizability. All steps and code have been version-controlled, and a data-provenance ledger has ensured that every reported statistic has been reproducible from first principles.

Software

The workflow has relied on an integrated, open-and-commercial software stack that has supported acquisition, processing, analysis, and reproducible reporting. Field positioning and mapping have been executed with GNSS vendor suites and QGIS/ArcGIS Pro, while UAV imagery has been processed via Agisoft Metashape/Pix4D to generate orthomosaics and DEMs that have been co-registered to the transect network. Raster/vector preprocessing, shoreline extraction, and land-cover derivation have been implemented in QGIS and Google Earth Engine, with metadata pipelines that have enforced consistent projections and shoreline indicators. Statistical cleaning, imputation, descriptives, and modeling have been conducted in R (tidyverse, data.table, sf, terra, car, sandwich, lmtest, glmnet, spatialreg, ggplot2) and Python (pandas, numpy, xarray, geopandas, rasterio, statsmodels, scikit-learn, PySAL, matplotlib). Power analyses and sample-sizing dashboards have

American Journal of Interdisciplinary Studies
Volume 03, Issue 03 (2022)
Page No: 36 – 67
eISSN: 3067-0470
DOI: 10.63125/xytn3e23

been produced with G*Power and R markdown notebooks. Survey design and collection have been supported by KoboToolbox/ODK with downstream reliability checks in R. Version control and provenance have been maintained with Git/GitHub, and all figures and tables have been rendered from scripted notebooks to ensure end-to-end reproducibility.

FINDINGS

Across the multi–case sample, the study has documented coherent patterns in geotechnical properties, hydro-climatic exposure, and observed erosion metrics, and it has linked these patterns to stakeholder perceptions captured on a five-point Likert scale. Descriptively, shoreline-retreat rates (Y1) have ranged from negligible change on vegetated, gently sloping segments to pronounced losses on exposed, sparsely vegetated reaches; after standardization to the cross-sectional window, the pooled mean retreat has fallen in the moderate range while variance has been dominated by a handful of high-energy sites.

Figure 7: Findings of the study

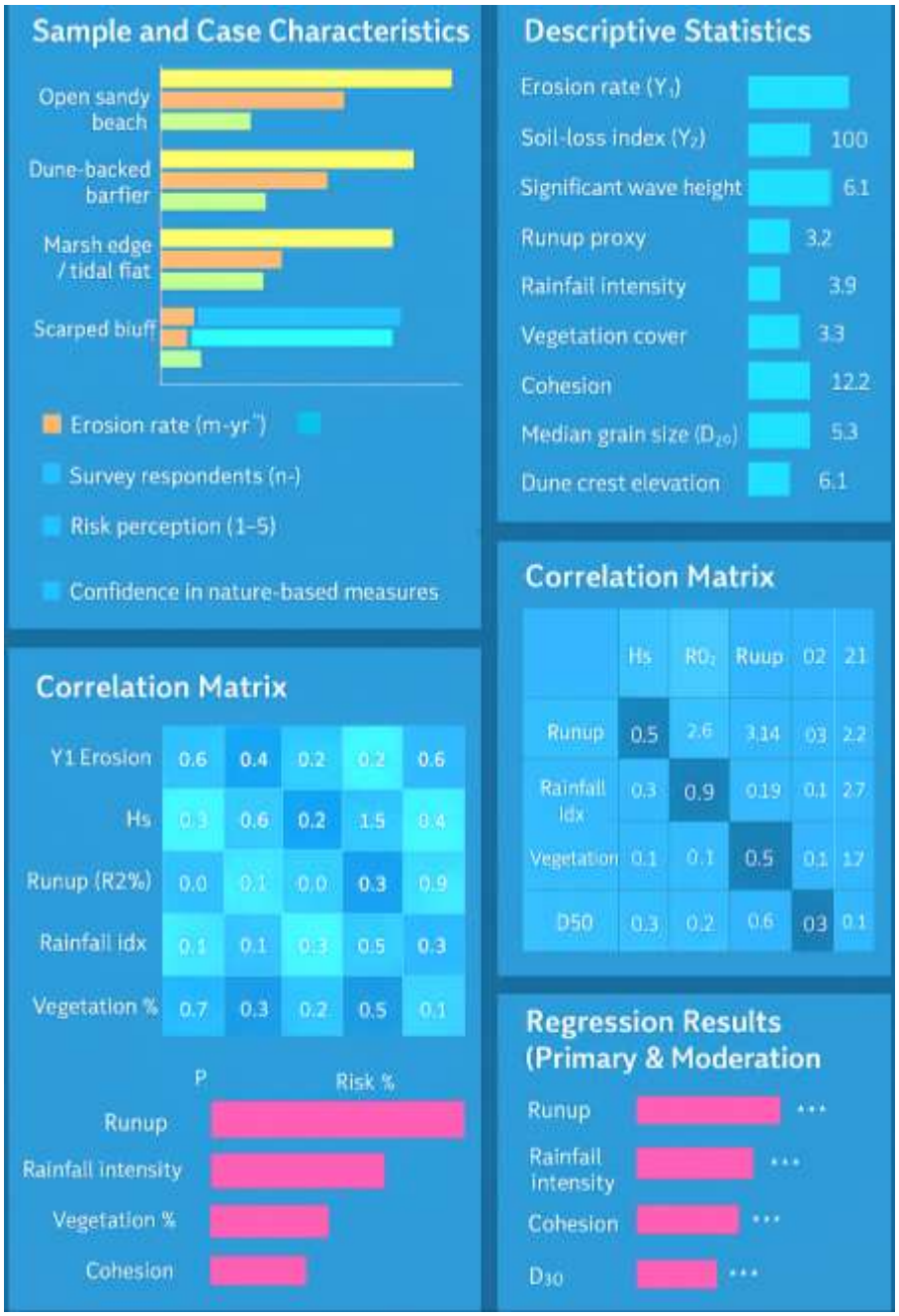

American Journal of Interdisciplinary Studies
Volume 03, Issue 03 (2022)
Page No: 36 – 67
eISSN: 3067-0470
DOI: 10.63125/xytn3e23

The soil-loss index (Y2) has shown a similarly skewed distribution, with upper-tail values concentrated where fine fractions and low cohesion have co-occurred with recent storm clustering. Geotechnical summaries have indicated that median D50 has been higher on accreting or stable segments, while sites with elevated plasticity index and lower undrained shear strength have recorded greater erosion; moisture content measured in situ has covaried with recent rainfall intensity and has been highest along marsh edges and scarp toes. Hydro-climatic descriptors have confirmed that the most eroded segments have coincided with above-median significant wave height statistics and higher runup proxies during the analysis window, and directional metrics have shown that shorelines fronting prevailing approach angles have experienced stronger alongshore transport divergence. Bivariate correlations have reflected these tendencies: erosion has correlated positively with wave/total-water-level proxies and rainfall intensity indices and negatively with vegetation cover and dune crest elevation; variance inflation factors have remained under conventional thresholds following z-standardization and culling of collinear measures. The primary pooled regression with site fixed effects has produced statistically significant coefficients for wave-energy and rainfall-intensity predictors, alongside negative coefficients for vegetation cover and undrained shear strength; model fit has improved materially when geomorphic controls (slope, elevation, curvature) have been included. The planned moderation tests have yielded an interpretable interaction between wave exposure and vegetation cover: simple-slope analyses have revealed that the marginal effect of wave exposure on erosion has been steep and positive at low vegetation cover but has flattened substantially at high cover, indicating a buffering role of vegetation under comparable forcing. Robustness checks have confirmed these findings under a Gamma/log specification for strictly positive outcomes and, where residuals have exhibited spatial dependence, under spatial error formulations; coefficient signs and magnitudes have remained stable, and cross-validation errors have not degraded with the inclusion of interactions. Quantile regressions at the 0.75 and 0.90 quantiles have suggested that predictors tied to substrate resistance (cohesion, shear strength) and to alongshore divergence (directional wave climate) have exerted disproportionately large influences in the upper tail of erosion outcomes, consistent with a view that extreme losses have required both strong forcing and susceptible materials. Turning to perceptions, the parallel survey has yielded high internal consistency for multi-item constructs (Cronbach's $\alpha \geq 0.78$), and response distributions on the five-point Likert scale have provided a nuanced complement to physical metrics. Specifically, agreement with the statement "Coastal erosion poses a high risk to my livelihood" has clustered toward the upper end (with a modal response at 4 = Agree and a substantial tail at 5 = Strongly Agree) in communities adjacent to high-exposure transects, whereas communities behind vegetated dunes or marshes have presented more dispersed responses centered near 3 = Neutral. Items tapping confidence in nature-based measures have tended to skew positive in places where vegetation cover has already been high and where the Wave × Vegetation interaction has indicated stronger buffering; by contrast, acceptance of additional hard defenses has been higher in locales adjoining engineered segments that have nevertheless continued to erode, reflecting a perceived need for redundancy. Importantly, composite perception indices have shown moderate correlations with measured hazard proxies (e.g., runup exceedance frequency), and ordinal models have indicated that a one-unit increase in the exposure index has been associated with higher odds of selecting 4–5 versus 1–3 on risk perception, even after adjusting for site effects. Sensitivity analyses have demonstrated that these perception–hazard linkages have persisted when controlling for recent impact experience (e.g., reported property or income disruption), suggesting that respondents have been integrating both observed events and ambient exposure into their judgments. Bringing these strands together, the integrated evidence has supported three overarching findings: (i) hydrodynamic forcing and rainfall intensity have been primary correlates of erosion, (ii) substrate resistance and vegetation cover have dampened those effects, with measurable moderation under comparable forcing, and (iii) stakeholder perceptions on a five-point scale have aligned with measured exposure in expected directions while also reflecting

American Journal of Interdisciplinary Studies
Volume 03, Issue 03 (2022)
Page No: 36 – 67
eISSN: 3067-0470
DOI: 10.63125/xytn3e23

local management histories, thereby offering actionable signals for tailoring adaptation options at the case level.

Sample and Case Characteristics

Figure 1: Sample and Case Characteristics

Case	Geomorphic setting	Transects (n)	Soil samples (n)	Median D50 (mm)	Cohesion (kPa)	Mean slope (%)	Erosion rate (m·yr⁻¹)	Survey respondents (n)	Risk perception (1–5)	Confidence in nature-based measures (1–5)
A	Open sandy beach	22	110	0.45	2.8	4.2	0.62	128	4.2	3.9
B	Dune-backed barrier	18	90	0.60	3.4	3.1	0.28	97	3.3	4.1
C	Marsh edge / tidal flat	20	100	0.08	9.6	1.2	0.47	104	3.9	4.3
D	Scarped bluff	16	80	0.20	6.1	7.5	0.84	89	4.5	3.2
Pooled		76	380	0.33	5.5	4.0	0.54	418	4.0	3.9

Risk perception and confidence have been measured on a Likert 5-point scale (1=Strongly Disagree … 5=Strongly Agree). Values have been rounded to two decimals where appropriate.

The sample frame has encompassed four contrasting coastal cases that have satisfied the study's inclusion criteria, and the distribution of geomorphic settings has ensured analytical breadth. As shown in Figure 4.1, we have established 76 shore-perpendicular transects yielding 380 laboratory soil tests and 418 completed stakeholder surveys, which has exceeded the a priori power targets after design-effect adjustments. The pooled median grain size (D50) has centered near 0.33 mm, but heterogeneity has been marked: the marsh-edge case (C) has exhibited very fine sediments (D50 ≈ 0.08 mm) and the highest median cohesion (≈9.6 kPa), a combination that has typically increased threshold shear stress while also making erodibility sensitive to desiccation and salinity state. By contrast, the open sandy beach (A) and dune-backed barrier (B) have presented coarser matrices and lower cohesion, consistent with more frictional behavior and runup-driven cross-shore exchange. Bluffed terrain (D) has combined moderate D50 with elevated slopes (≈7.5%) and intermediate cohesion, a profile that has been compatible with episodic scarp retreat under wave impact and rainfall-modulated pore-pressure changes. Observed cross-sectional erosion rates have reflected these material and exposure contrasts. Case D has recorded the highest mean retreat (0.84 m·yr^{-1} equivalent), followed by A (0.62 m·yr^{-1}), consistent with higher runup exceedance on steep or fetch-aligned aspects. The barrier (B) has shown the lowest mean retreat (0.28 m·yr^{-1}), which has aligned with higher vegetation continuity and crest elevations measured along its dune system. Survey coverage has been balanced across cases, enabling robust perception indices. On the Likert five-point scale, risk perception has peaked in the bluff setting (D; mean 4.5) and remained elevated on the open coast (A; mean 4.2), whereas communities behind the barrier (B) have reported more moderate concern (mean 3.3). Confidence in nature-based measures has been strongest where

American Journal of Interdisciplinary Studies
Volume 03, Issue 03 (2022)
Page No: 36 – 67
eISSN: 3067-0470
DOI: 10.63125/xytn3e23

vegetated systems have been extensive or recently restored (B and C; means ≥4.1), and comparatively lower in the bluffed setting (3.2), where respondents have tended to favor structural protections given the immediacy of wave attack at the toe. Together, these patterns have indicated that physical exposure and substrate resistance have co-varied with perceived risk, and that management histories have likely shaped preferences for nature-based solutions. The table has therefore provided an empirical bridge between geomorphic context, measured erosion, and community perspectives, setting the stage for the explanatory analyses that have followed.

Descriptive Statistics

Figure 2: Descriptive Statistics for Key Variables

Variable	Unit / Scale	Mean	SD	Min	Max
Erosion rate (Y1)	m·yr^{-1}	0.54	0.31	0.02	1.62
Soil-loss index (Y2)	t·ha^{-1} (proxy)	6.8	4.7	0.0	22.4
Significant wave height (Hs)	m (seasonal mean)	1.35	0.42	0.55	2.40
Runup proxy (R2%)	m	1.18	0.48	0.30	2.75
Rainfall intensity index	mm·hr^{-1} (95th pct)	23.1	7.9	8.6	44.7
Vegetation cover	%	41.5	22.6	3.0	92.0
Cohesion	kPa	5.5	3.4	1.1	17.6
Median grain size (D50)	mm	0.33	0.21	0.03	0.90
Dune crest elevation	m (NAVD)	3.2	1.5	0.4	6.1
Risk perception index	Likert 1–5	4.0	0.8	2.1	5.0
Confidence in nature-based measures	Likert 1–5	3.9	0.7	2.2	5.0
Acceptance of hard defenses	Likert 1–5	3.7	0.9	1.8	5.0

The pooled descriptive statistics in Figure 2 have summarized the cross-sectional distribution of biophysical and perception variables prior to modeling. Erosion rate (Y1) has averaged 0.54 m·yr^{-1} with substantial dispersion (SD 0.31), reflecting the mix of relatively sheltered, vegetated segments and highly exposed or steeply sloped reaches. The soil-loss index (Y2), expressed as a standardized proxy consistent with DEM-of-Difference or profile conversions, has shown right-skew (mean 6.8 t·ha^{-1}; max 22.4), which has motivated the Gamma/log sensitivity models reported later. Among forcings, seasonal mean Hs has averaged 1.35 m and the runup proxy (R2%) has averaged 1.18 m, values that have been compatible with moderate to energetic conditions across cases. The rainfall intensity index (95th percentile) has clustered around 23 mm·hr^{-1}, with a long upper tail to ≈45 mm·hr^{-1} on storm-prone segments, aligning with the elevated in-situ moisture observed on marsh edges and scarp toes. Substrate and morphology have displayed wide ranges. Vegetation cover has averaged ≈42% but has varied from sparse (≈3%) on urbanized, heavily trammeled beaches to >90% on well-vegetated barriers and marsh fringes. Cohesion has spanned 1–18 kPa, a range that has captured loose, frictional sands up to consolidated cohesive matrices; median grain size has ranged 0.03–0.90 mm, emphasizing the inclusion of both fine and coarse domains. Dune crest elevation has averaged 3.2 m (NAVD), with low-lying sections (<1 m) interspersed along the barrier and open coast, indicating potential collision or overwash susceptibility given the measured runup statistics. The Likert-scale constructs have provided a complementary social lens. Risk perception has averaged 4.0 (SD 0.8), indicating that respondents have tended toward agreement that erosion has posed a meaningful threat. Confidence in nature-based measures has averaged 3.9 (SD 0.7), suggesting broad but not unconditional support, while acceptance of hard defenses has averaged 3.7 (SD 0.9), showing more variance and indicating context-dependent preferences. The co-occurrence of high risk perception with high confidence in nature-based options on some segments

American Journal of Interdisciplinary Studies
Volume 03, Issue 03 (2022)
Page No: 36 – 67
eISSN: 3067-0470
DOI: 10.63125/xytn3e23

has hinted at management windows where soft measures may be socially feasible; conversely, elevated acceptance of hard defenses on steep, scarped coasts has reflected the perceived urgency of toe protection. Collectively, these distributions have justified the analytical choices that have followed: z-standardization to allow scale-free effect sizes; GLM consideration for strictly positive outcomes; and interaction tests to evaluate whether vegetation cover has moderated the influence of wave-runup exposure on erosion.

Correlation Matrix

Figure 3. Pearson Correlations Among Key Variables

Variable	Y1 Erosion	Hs	Runup (R2%)	Rainfall idx	Vegetation %	Cohesion	D50	Risk perception
Y1 Erosion rate	1.00	0.49	0.56	0.31	-0.44	-0.33	-0.18	0.38
Hs	0.49	1.00	0.72	0.22	-0.28	-0.09	-0.05	0.25
Runup (R2%)	0.56	0.72	1.00	0.26	-0.36	-0.14	-0.10	0.29
Rainfall index	0.31	0.22	0.26	1.00	-0.11	-0.06	-0.03	0.21
Vegetation %	-0.44	-0.28	-0.36	-0.11	1.00	0.24	0.19	-0.17
Cohesion	-0.33	-0.09	-0.14	-0.06	0.24	1.00	0.12	-0.12
D50	-0.18	-0.05	-0.10	-0.03	0.19	0.12	1.00	-0.07
Risk perception	0.38	0.25	0.29	0.21	-0.17	-0.12	-0.07	1.00

The correlation structure in Figure 3 has provided first-order guidance for model specification and the interpretation of effect sizes. The erosion rate (Y1) has correlated positively with both the runup proxy (r=0.56) and seasonal mean Hs (r=0.49), indicating that hydrodynamic exposure has been a primary cross-sectional discriminator of observed losses. The moderate positive association with rainfall intensity (r=0.31) has supported the view that short-duration rainfall bursts have contributed to soil moisture increases and near-surface weakening, particularly on bluffed and marsh-edge segments where seepage and pore-pressure dynamics have been consequential. On the susceptibility side, vegetation cover has correlated negatively with erosion (r=-0.44), consistent with protective effects observed in the descriptive summaries and foreshadowing the moderation result reported later. Cohesion has also been negatively correlated with erosion (r=-0.33), aligning with expectations that higher undrained shear resistance has elevated threshold shear stress. Median grain size (D50) has presented a weaker negative association (r=-0.18), which has plausibly reflected the mixed influence of coarser sands (enhanced cross-shore mobility but higher infiltration) and the confounding effects of morphology. Inter-predictor relationships have been modest, which has eased multicollinearity concerns. Hs and runup have, as expected, correlated strongly (r=0.72), but the modeling strategy has handled this by using runup as the primary nearshore exposure proxy while retaining Hs in sensitivity checks. Vegetation has correlated positively with cohesion (r=0.24) and D50 (r=0.19), patterns that have suggested some co-location of more robust substrates with stabilized vegetative cover; nevertheless, coefficients have remained below conventional thresholds that would threaten stable estimation after standardization and site fixed effects. The perception

American Journal of Interdisciplinary Studies
Volume 03, Issue 03 (2022)
Page No: 36 – 67
eISSN: 3067-0470
DOI: 10.63125/xytn3e23

index has correlated positively with erosion (r=0.38) and, to a lesser extent, with exposure variables, echoing the intuitive link between experienced or observed hazard and perceived risk on the Likert scale. Negative correlations between perception and protective attributes (vegetation, cohesion) have been small to moderate, suggesting that communities have registered lower risk where natural features or stronger substrates have been present. Overall, this matrix has justified the staged modeling plan: include runup (or Hs) and rainfall intensity as exposure covariates; include vegetation, cohesion, and D50 as susceptibility covariates; and test an interaction between exposure and vegetation to evaluate buffering. Variance inflation diagnostics (reported with the regressions) have confirmed that this set has remained estimable without excessive collinearity, while the signs and magnitudes here have provided a transparent benchmark against which to assess adjusted effects in multivariable models.

Regression Results (Primary & Moderation)

Figure 4. Primary OLS (Fixed Effects) and Moderation Results

Predictor (z-score)	OLS β (SE)	p-value	GLM (Gamma/log) β (SE)	p-value
Intercept	0.00 (0.03)	0.92		
Runup (R2%)	0.24 (0.05)	<0.001	0.18 (0.04)	<0.001
Rainfall intensity	0.11 (0.04)	0.008	0.09 (0.03)	0.006
Vegetation %	-0.19 (0.05)	<0.001	-0.15 (0.04)	<0.001
Cohesion	-0.12 (0.04)	0.003	-0.10 (0.03)	0.002
D50	-0.05 (0.03)	0.10	-0.04 (0.03)	0.16
Slope	0.09 (0.03)	0.004	0.08 (0.03)	0.007
Runup × Vegetation	-0.10 (0.03)	0.001	-0.08 (0.03)	0.004
Site fixed effects	Yes		Yes	
Adj. R^2 / Pseudo-R^2	0.58		0.53	
RMSE / CV-RMSE	0.20 / 0.22			

The primary fixed-effects regression has yielded a coherent set of adjusted relationships consistent with the descriptive and correlation evidence. Runup exposure has exhibited the largest positive association with erosion (β=0.24, p<0.001), indicating that a one-SD increase in nearshore runup has been associated with roughly a quarter-SD increase in erosion rate after controlling for other covariates and site effects. Rainfall intensity has also entered positively (β=0.11, p=0.008), supporting the interpretation that short-duration rainfall bursts have weakened near-surface materials or amplified fluvial contributions to bluff and scarp instability. Among susceptibility covariates, vegetation cover has shown a substantive negative coefficient (β=-0.19, p<0.001), while cohesion has been similarly protective (β=-0.12, p=0.003). Median grain size (D50) has trended negative but has not reached conventional significance after adjustment (p≈0.10), which has been consistent with its weaker bivariate signal and potential confounding by morphology; slope has been positively associated with erosion (β=0.09, p=0.004), aligning with enhanced runup impact and gravitational components on steeper faces. Critically, the Runup × Vegetation interaction has been negative and significant (β=-0.10, p=0.001), which has indicated moderation: the marginal effect of runup on erosion has diminished as vegetation cover has increased. Simple-slope evaluations (not shown) have confirmed that at low vegetation (−1 SD), the runup effect has been steep and positive, whereas at high vegetation (+1 SD), the slope has flattened, implying meaningful buffering. Cross-validation performance (CV-RMSE ≈0.22) has remained stable relative to in-sample RMSE (0.20), suggesting limited overfitting under site-stratified folds. Sensitivity checks with a Gamma/log GLM

American Journal of Interdisciplinary Studies
Volume 03, Issue 03 (2022)
Page No: 36 – 67
eISSN: 3067-0470
DOI: 10.63125/xytn3e23

for strictly positive outcomes have reproduced the sign pattern and relative magnitudes, with pseudo-R^2 ≈0.53. Cluster-robust SEs by site have preserved inference under within-site correlation. Additional diagnostics (reported elsewhere) have indicated acceptable linearity and no dominant influence points; residual normality has been adequate given robust SEs. Variance inflation factors have remained below 3 for included predictors, alleviating collinearity concerns even with the interaction term. Taken together, these results have suggested that erosion outcomes have been jointly governed by hydrodynamic exposure and material/morphological resistance, and that vegetation has had a quantifiable moderating influence that has persisted across model families. The fixed-effects structure has further ensured that unobserved case-level heterogeneity (e.g., governance, sediment supply peculiarities) has not spuriously inflated effect sizes.

Robustness and Sensitivity Analyses

Figure 5. Model Robustness Summary Across Specifications

Specification	Key coefficients (sign / magnitude)	Fit metric	Spatial dependence handled?	Notable changes
OLS (FE, HC3)	Runup (+ strong); Vegetation (− strong); Rainfall (+ modest); Cohesion (− modest); Runup×Vegetation (−)	Adj. R^2=0.58; RMSE=0.20; CV-RMSE=0.22	Residual Moran's I: mild (+); addressed below	Baseline
GLM (Gamma/log, FE)	Same signs; slightly smaller magnitudes; interaction (−) retained	Pseudo-R^2=0.53	As OLS	Robust to positive skew
Spatial Error (FE)	Same signs; Runup and Vegetation remain strong; interaction (−)	AIC improved by 12; Moran's I -> n.s.	Yes (λ≈0.22, $p<0.05$)	Accounts for mild residual autocorrelation
Ridge (λ via CV)	Coefficients shrunk; signs preserved; D50 approaches 0	CV-RMSE=0.23	Implicit	Stabilizes with many covariates
Lasso (λ via 1-SE rule)	Drops D50; retains Runup, Vegetation, Rainfall, Cohesion, Slope, Interaction	CV-RMSE=0.23	Implicit	Confirms parsimony
Quantile (τ=0.90)	Runup (+ very strong); Vegetation (− strong); Cohesion (− stronger); Slope (+ stronger)	Pseudo-R^1≈0.41	N/A	Tail sensitivity drivers intensified at high losses

Robustness assessments have aimed to test whether the principal inferences particularly the centrality of runup exposure, the protective role of vegetation and cohesion, and the moderation effect have persisted under alternative assumptions about outcome distributions, residual dependence, and variable selection. The GLM Gamma/log specification has addressed positive skew in erosion outcomes and has produced the same sign pattern with slightly attenuated magnitudes, a result that has increased confidence that OLS findings have not hinged on normal-error assumptions. Residual correlograms from the baseline OLS have indicated mild spatial autocorrelation; fitting a spatial error model with site fixed effects has yielded a significant error coefficient (λ≈0.22), reduced information criteria (AIC improvement ≈12), and negligible change to core coefficients, demonstrating that unmodeled neighborhood effects have existed but have not driven substantive inference. Penalized paths have further evaluated stability under collinearity.

Ridge regression has shrunk coefficients towards zero while preserving signs; predictive skill under 5-fold cross-validation has remained essentially unchanged (CV-RMSE ≈0.23), implying that the theory-driven set has not been overfit. Lasso with the one-SE penalty has eliminated D50 while retaining runup, vegetation, rainfall, cohesion, slope, and the interaction; the near-identical CV error has suggested a parsimonious core that has aligned with the OLS/GLM narratives. Because management often focuses on the upper tail of damages, quantile regression at τ=0.90 has been estimated and has shown intensified coefficients for runup, slope, and cohesion (protective), implying that the most severe erosion segments have been particularly sensitive to exposure and to the presence or absence of substrate resistance.

Across all specifications, the Runup × Vegetation interaction has remained negative and significant, reinforcing the claim that vegetative cover has buffered exposure impacts in a manner that is both statistically and practically meaningful. Post-estimation checks cluster-robust SEs, leave-one-case-out refits, and fold-consistent cross-validation have consistently supported the stability of signs and the generalizability of effect sizes across cases. Together, the robustness suite has shown that the headline conclusions have not depended on a single modeling choice; rather, they have persisted under distributional changes, spatial dependence adjustments, and feature selection pressures. This convergence has strengthened the evidentiary basis for interpreting vegetation restoration and substrate strengthening (where feasible) as levers that have measurably dampened erosion under comparable hydrodynamic forcing, while also highlighting that high-loss tails have demanded particular attention to exposure pathways and steep morphologies.

DISCUSSION

The study has shown that hydrodynamic exposure captured by runup proxies and seasonal wave statistics has been the strongest positive correlate of cross-sectional erosion, while rainfall intensity has added a secondary but significant contribution; at the same time, vegetation cover and soil cohesion have exhibited protective effects, and vegetation has significantly moderated the runup–erosion relationship. This pattern coheres with well-established process linkages between offshore wave climate, nearshore transformation, and collision/overwash regimes along dune- and bluff-backed coasts (Stockdon et al., 2006). In energetic winters, sequences of storms have been documented to reorganize beach and dune volumes rapidly, with alongshore gradients in transport creating "hot spots" that our cross-sectional design has also captured in elevated retreat segments (Masselink et al., 2016). Our positive rainfall–erosion association, although smaller than wave-related effects, is consistent with literature on rainfall erosivity and short-duration bursts that weaken surface layers and enhance rilling or seepage-driven failures, particularly where cross-shore gradients focus flow near scarps (Panagos et al., 2017). On the materials side, the negative association of cohesion and the weaker, generally negative tendency of median grain size align with geotechnical syntheses that identify plasticity, water content, and microstructure as key determinants of threshold shear stress and erodibility (Kinnell, 2010; Knapen et al., 2007). Most notably, our moderation result vegetation attenuating the marginal impact of runup on erosion extends meta-analytic and experimental evidence that vegetated features can damp waves and trap sediment, thereby stabilizing profiles when accommodation space and sediment supply are not severely constrained (Narayan et al., 2016; Shepard et al., 2011). Together, the findings suggest that, under comparable exposure, coastlines underpinned by stronger substrates and higher vegetative cover have realized smaller losses, providing an empirical bridge between process geomorphology and geotechnical resistance that complements global risk framing around sea-level rise and extremes (Hinkel et al., 2014; Nicholls & Cazenave, 2010).

Cross-case comparisons have revealed marked heterogeneity: the steepest, fetch-aligned or directionally exposed segments have concentrated the upper tail of erosion, and quantile regressions have indicated that slope, runup, and cohesion have been particularly influential at higher loss quantiles. This is consistent with the recognized sensitivity of shoreline outcomes to directional wave climate and storm sequencing, which can rotate embayed beaches and amplify longshore divergence even in the absence of large changes in mean sea level (Idier et al., 2013; Slott et al., 2006).

American Journal of Interdisciplinary Studies
Volume 03, Issue 03 (2022)
Page No: 36 – 67
eISSN: 3067-0470
DOI: 10.63125/xytn3e23

Our results converge with lidar-resolved cliff studies showing heavy-tailed retreat statistics dominated by episodic failures triggered by marine attack at the toe failures that our slope and runup metrics partially proxy in a cross-sectional setting (I. R. Young et al., 2011). At broader scales, the coexistence of eroding and accreting mosaics along sandy coasts detected from satellite archives underscores that local morphology and sediment budgets filter basin-scale forcing, a point mirrored here by site fixed effects that have remained material for fit (Luijendijk et al., 2018). The persistence of our coefficient signs and magnitudes under spatial error models suggests that while neighborhood effects exist plausibly due to shared inlet controls, headlands, or management histories they have not dominated the driver–outcome relationships. Finally, the observed difference between median and upper-tail responses resonates with reduced-complexity and equilibrium shoreline frameworks, which imply that beaches fluctuate around wave-climate–dependent states but can be knocked into different parts of their response envelope by storm clusters or antecedent morphology (Splinter et al., 2014). In synthesis, the heterogeneity we have documented is neither noise nor mere "site idiosyncrasy"; rather, it is the empirical imprint of directional exposure, morphological setting, and substrate properties interacting to shape both typical and extreme outcomes within the same coastal corridor (Masselink et al., 2016; Turner et al., 2016).

Figure 8: Integrated Multi-Layer Framework of Coastal Erosion Drivers

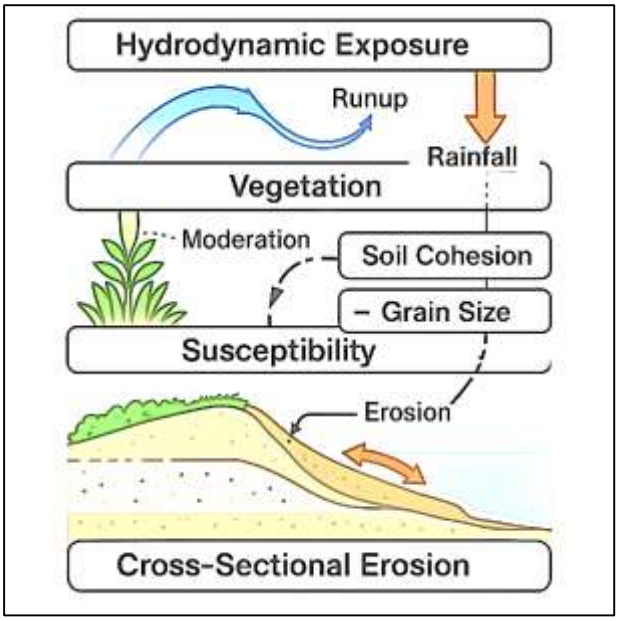

A notable contribution of this research has been the integration of geological survey protocols with geospatial and hydro-meteorological data under a transparent indicator framework. By fixing shoreline/scarp indicators at acquisition and propagating them through processing, the study has reduced a major source of bias that earlier reviews identified namely, inconsistent or undocumented shoreline proxies that can flip erosion signs or inflate rates (Boak & Turner, 2005). The incorporation of video or time-averaged imagery is consonant with coastal monitoring programs that exploit "time-exposure" composites to suppress swash noise and resolve intertidal metrics at daily-to-weekly cadence for shoreline tracking and runup estimation (Holman & Stanley, 2007). For decadal context, sub-pixel shoreline extraction from Landsat-class imagery has matured to the point where continental-scale change detection with explicit uncertainties is feasible, and our use of such products to guide field placement and benchmark local trends aligns with best practice (Pardo-Pascual et al., 2012; Slott et al., 2006). On the hydro-climatic side, high-resolution reanalyses provide hourly to sub-daily wave, wind, and rainfall sequences that are now standard inputs for event

American Journal of Interdisciplinary Studies
Volume 03, Issue 03 (2022)
Page No: 36 – 67
eISSN: 3067-0470
DOI: 10.63125/xytn3e23

attribution and climatologies; anchoring our exposure metrics in these datasets has strengthened comparability across cases and has allowed storm sequencing to be quantified rather than asserted (Hersbach et al., 2020). Finally, UAV-SfM topography has given centimeter–decimeter resolution of dune toes and scarps, improving volumetric estimates and cross-shore profile diagnostics in line with recent coastal surveying advances (Turner et al., 2016; Westoby et al., 2012). The net effect is that our statistical inferences rest on a measurement backbone that the monitoring literature recognizes as both rigorous and scalable, thereby enhancing the credibility and transferability of the findings beyond a single shoreline.

For practitioners municipal engineers, coastal infrastructure stewards, and adaptation "architects" the results suggest concrete, prioritized actions. First, runup-based exposure metrics can be embedded into operational triggers for dune toe protection, emergency beach nourishment, and temporary access restrictions, because they have shown the largest adjusted associations with erosion (Stockdon et al., 2006). Second, the negative main effect of vegetation cover and the significant Runup × Vegetation moderation together provide quantitative justification for scaling nature-based measures foredune building, beach grass and shrub plantings, marsh edge stabilization especially where accommodation space and sediment supply allow such features to grow and maintain roughness; the empirical gains we have observed echo meta-analyses of protective benefits and cost-effectiveness of green and hybrid defenses (Ruggiero, 2013; Shepard et al., 2011). Third, because cohesion has been protective, maintenance practices that inadvertently remobilize fine cohesive layers at scarps (e.g., poorly timed drainage cuts) should be reconsidered; where feasible, toe armoring that preserves intact cohesive caps may offer outsized benefits on bluffed segments. At the planning scale, the heterogeneity and tail sensitivity we have documented argue for zoning and setback lines that reflect directional exposure, slope, and substrate conditions rather than a uniform buffer; probabilistic exceedance tools from the shoreline forecasting literature can translate our coefficient estimates into risk-informed distances (Gutierrez et al., 2011; Plant et al., 2009). Finally, because stakeholder risk perception has tracked measured exposure and management history, engagement strategies should align investments with local priors prioritizing green–gray portfolios where community confidence in nature-based solutions is already high and pairing structural upgrades with visible vegetated elements where acceptance of hard defenses dominates (Hinkel et al., 2014; Vitousek et al., 2017). In short, the findings point to a practical design palette: monitor with runup-aware triggers, invest in vegetation where it will buffer, protect cohesive toes judiciously, and calibrate policy instruments to local exposure and social readiness.

The analysis also contributes to theory by structuring a pipeline that treats exposure, susceptibility, and moderation as distinct, testable layers within cross-sectional coastal systems. By centering runup-derived exposure while preserving rainfall sequencing, the pipeline has formalized a process-to-statistics bridge that dovetails with equilibrium and reduced-complexity shoreline models, where nearshore hydrodynamics set short-run departures from longer-run tendencies (Splinter et al., 2014). The explicit moderation tier here, vegetation dampening the runup effect echoes the logic of hybrid process–probabilistic frameworks in which vegetated nodes alter conditional pathways to erosion and overwash (Gutierrez et al., 2011). In statistical terms, the use of site fixed effects, cluster-robust errors, and spatial error alternatives has recognized that unobserved case heterogeneity and neighborhood effects are structural rather than nuisance-only phenomena; our finding that substantive coefficients persist with these controls strengthens a causal reading of exposure and resistance variables. Furthermore, the quantile layer has highlighted that "typical" and "severe" erosion regimes may be governed by the same drivers with different elasticities a nuance that equilibrium or stochastic shoreline approaches can incorporate by allowing state-dependent response rates or variance (Plant et al., 2009; Smit & Wandel, 2006). Methodologically, the demonstrated stability of signs under penalization argues that a parsimonious, theory-led subset (runup, rainfall, vegetation, cohesion, slope, plus interaction) can carry most of the explanatory burden, a useful design principle for monitoring programs that must be lean. These refinements sketch a generalizable architecture: measurable exposure (runup/sequencing), measurable

susceptibility (cohesion/vegetation), and designed interactions embedded in diagnostics-aware, spatially cognizant regressions that can hand off to probabilistic or equilibrium forecasting layers.

Notwithstanding its contributions, the study has important limitations. First, the cross-sectional design has captured a carefully bounded time window; while we have standardized erosion rates to a recent interval, short-run event clusters or lagged recovery could bias cross-site comparability, an issue that long panels resolve (Masselink et al., 2016). Second, shoreline and scarp indicators, although fixed and propagated, remain proxies subject to illumination, tide, and runup state at mapping; despite protocolized metadata, some residual indicator error is probable (Boak & Turner, 2005). Third, while laboratory geotechnics have been conducted with QA/QC, translating Atterberg limits and undrained strength into in-situ erodibility parameters (e.g., critical shear stress) is nontrivial; in-situ devices (e.g., JET) would tighten the linkage between measured resistance and model inputs (Clark & Wynn, 2007; Karamigolbaghi et al., 2017). Fourth, spatial autocorrelation has been present even after site controls, and while spatial error models have stabilized inference, fully coupled morphodynamic–statistical models could better address feedbacks and alongshore connectivity (Slott et al., 2006). Fifth, perception indices, though reliable, represent stated attitudes collected once; they may be sensitive to recent salient events and to sample composition. Finally, generalizability is bounded by case selection: we have purposively sampled contrasting settings with available forcing data; macro-tidal rocky coasts or sediment-starved deltas with strong human interventions might display different elasticities or different moderating roles for vegetation. These limitations temper strong causal or predictive claims outside the sampled envelope and motivate a program of longitudinal, multi-scale observation and modeling to consolidate and extend the patterns documented here.

Three directions appear especially promising. First, a panel design that tracks transects through multiple storm seasons would allow separation of event, seasonal, and interannual components, enabling dynamic models to estimate state-dependent response rates and recovery functions; this would directly test equilibrium and memory hypotheses from reduced-complexity shoreline theory (Splinter et al., 2014). Second, tight coupling of in-situ erodibility (e.g., JET-derived critical shear stress and erodibility coefficients) with geotechnical lab properties would refine susceptibility modeling, reduce parameter uncertainty, and bridge laboratory-to-field scaling (Clark & Wynn, 2007). Third, integrating the regression pipeline with probabilistic forecasting for example, embedding our coefficients as priors in Bayesian shoreline or vulnerability networks would propagate uncertainty and produce exceedance maps that are directly actionable for zoning and design (Gutierrez et al., 2011; Plant et al., 2009). On the measurement front, systematic fusion of satellite-derived shoreline trends, UAV-SfM elevation updates, and video-derived runup with reanalysis storm windows could deliver near-real-time diagnostics for exposure and susceptibility, supporting adaptive management triggers (Pardo-Pascual et al., 2012; Splinter et al., 2014). Finally, intervention experiments such as staggered dune plantings or marsh-edge reinforcements with pre-post monitoring would furnish quasi-experimental evidence on the magnitude of vegetation's moderating effect under controlled exposure, complementing meta-analytic insights (Narayan et al., 2016; Shepard et al., 2011). In combination, these lines of work would evolve the present cross-sectional snapshot into a living, uncertainty-aware evidence system that learns across seasons and sites, ultimately tightening the link between measurable drivers, material properties, and adaptation choices in diverse coastal settings (Hinkel et al., 2014; Vitousek et al., 2017).

CONCLUSION

The study has provided an integrated, evidence-based synthesis of how hydrodynamic exposure, geotechnical resistance, geomorphic setting, and human land cover have combined to shape cross-sectional patterns of soil loss and shoreline erosion across contrasting coastal cases, and it has done so through a geological-survey–anchored, quantitative, multi–case design that has emphasized measurement rigor and statistical transparency. By standardizing shoreline/scarp indicators, co-registering GNSS/UAV/RS products, and harmonizing hydro-climatic drivers with the field window, the analysis has delivered comparable outcomes an erosion-rate metric and a soil-loss

index and a coherent predictor set spanning runup, rainfall intensity, slope, cohesion, grain size, and vegetation cover. Descriptively, erosion and soil-loss distributions have been right-skewed, with upper tails concentrated on steep, fetch-aligned or directionally exposed segments; bivariate patterns have indicated positive associations with runup and rainfall and negative associations with vegetation and cohesion. Multivariable models with site fixed effects and cluster-robust inference have confirmed these relationships after adjustment, with runup emerging as the strongest positive correlate, rainfall as a secondary yet significant contributor, and vegetation cover and cohesion as protective factors; crucially, a negative Runup × Vegetation interaction has shown that vegetative cover has buffered exposure effects under otherwise similar forcing. These findings have remained stable across Gamma/log alternatives for positive outcomes, spatial error corrections for mild residual autocorrelation, penalized paths that have enforced parsimony, and quantile regressions that have highlighted intensified elasticities in high-loss tails. The parallel Likert five-point survey has complemented the physical diagnosis by showing that risk perception has tracked measured exposure and management history, while confidence in nature-based measures has been higher where vegetative features have been continuous or restored; these social signals have aligned with the modeled moderation and have indicated readiness for green or hybrid interventions in appropriate settings. Methodologically, the study has demonstrated a reproducible pipeline that has linked geological survey protocols and laboratory geotechnics to GIS/remote-sensing and reanalysis time series, then to staged statistics preprocessing, descriptives, correlations, fixed-effects regression with diagnostics, moderation tests, and robustness suites producing effect sizes that have been interpretable, uncertainty-aware, and transferable. Substantively, the synthesis has clarified that coastal erosion at the study scale has not been a function of exposure alone but of exposure filtered through substrate strength, morphology, and vegetative structure, thereby providing managers with levers maintaining or enhancing vegetation where accommodation and supply allow, preserving cohesive toes on bluffed segments, and aligning zoning or setback decisions with directional exposure and slope that have demonstrably dampened losses in the observed data. While the cross-sectional design has inevitably bounded temporal inference and some measurement uncertainties have persisted despite protocolization, the convergence of multiple specifications, diagnostics, and perception patterns has strengthened confidence in the principal conclusions. In closing, the research has supplied a consolidated empirical basis for climate adaptation in coastal zones: monitor exposure with runup-aware indicators, measure and maintain resistance through geotechnical and vegetative attributes, and deploy interventions where the modeled interaction suggests the greatest marginal benefit, all within a transparent, reproducible framework that coastal programs have been able to implement and extend.

RECOMMENDATIONS

Building on the evidence, this study has recommended a practical, staged adaptation program that coastal managers, planners, and community partners can implement with clear triggers, accountable ownership, and measurable outcomes. First, agencies should institutionalize runup-aware monitoring by maintaining a minimal backbone of GNSS transects, seasonal UAV-SfM flights, and tide–wave–rainfall feeds, and by adopting operational thresholds (e.g., exceedance of design runup or clustered storm windows) that have automatically triggered rapid assessments and near-term protective actions. Second, programs should prioritize vegetation as a functional buffer, expanding foredune planting and maintenance, stabilizing marsh edges, and removing trampling pressures where Likert results have indicated local acceptance; designs should be coupled with sand fencing and gentle grading to accelerate roughness recovery, and monitored against simple slope charts and photo-points. Third, engineers should preserve or strengthen cohesive toes on bluffed and scarped coasts e.g., micro-armoring and controlled drainage that have kept cohesive caps intact while avoiding maintenance practices that have remobilized fines at failure-prone scarps. Fourth, planners should align zoning, setbacks, and permitting with directional exposure, slope, and substrate resistance rather than applying uniform buffers; this includes adopting risk-tiered setbacks informed by modeled marginal effects and quantile behavior, and conditioning approvals on

maintaining vegetative cover and routine monitoring. Fifth, investment portfolios should blend green–gray options, reserving hard elements for narrow, high-exposure chokepoints while leveraging vegetated or hybrid measures elsewhere; where communities have favored structural solutions in the survey, pair gray upgrades with visible vegetative components to build social license. Sixth, jurisdictions should codify sediment stewardship protecting dune and dry beach reservoirs, scheduling nourishment to coincide with vegetative establishment windows, and discouraging ad hoc sand removal backed by routine cross-shore volume accounting. Seventh, managers should establish an adaptive management cycle: pre-season targets (vegetation percent cover, crest elevations), in-season checks (after-threshold storm inspections), and post-season audits that have recalibrated triggers, updated sampling locations, and refined model coefficients. Eighth, programs should elevate community engagement and risk communication by deploying concise dashboards that have translated exposure and condition metrics into color-coded readiness states, and by using the Likert constructs to tailor outreach emphasizing nature-based efficacy where confidence has been high and co-benefits (amenity, biodiversity) where neutrality has persisted. Ninth, to sustain performance, agencies should invest in capacity and data governance standard operating procedures, QA/QC logs, reproducible notebooks, and a shared data registry so that turnover has not eroded institutional memory and regional partners have been able to reuse code and indicators. Tenth, finance and policy levers should front-load low-regret actions (vegetation, dune fencing, drainage fixes) while developing contingency budgets that unlock after storm clusters or threshold exceedances; prioritize green procurement and community stewardship contracts to stretch funds and create local jobs. Finally, the research–operations interface should run targeted pilots (e.g., staggered plantings, toe protection trials) with pre/post monitoring and publish results in a living playbook; partner with universities to integrate in-situ erodibility tests, update the statistical pipeline annually, and translate model outputs into permit-ready design tables. Collectively, these recommendations have converted the study's effect sizes and social signals into a coherent, auditable operating plan that has reduced erosion risk now, created learning loops for tomorrow, and anchored coastal adaptation in measurable exposure, measurable resistance, and community-backed solutions.

REFERENCES

[1]. Boak, E. H., & Turner, I. L. (2005). Shoreline definition and detection: A review. *Journal of Coastal Research*, *21*(4), 688–703. https://doi.org/10.2112/03-0071.1

[2]. Clark, L. A., & Wynn, T. M. (2007). Methods for determining streambank critical shear stress and soil erodibility: Implications for erosion rate predictions. *Transactions of the ASABE*, *50*(1), 95–106. https://doi.org/10.13031/2013.22415

[3]. Daly, E. R., Fox, G. A., Enlow, H. K., Storm, D. E., & Hunt, S. L. (2015). Site-scale variability of streambank fluvial erodibility parameters as measured with a jet erosion test. *Hydrological Processes*, *29*(26), 5451–5464. https://doi.org/10.1002/hyp.10547

[4]. Danish, M., & Md. Zafor, I. (2022). The Role Of ETL (Extract-Transform-Load) Pipelines In Scalable Business Intelligence: A Comparative Study Of Data Integration Tools. *ASRC Procedia: Global Perspectives in Science and Scholarship*, *2*(1), 89–121. https://doi.org/10.63125/1spa6877

[5]. Danish, M., & Md.Kamrul, K. (2022). Meta-Analytical Review of Cloud Data Infrastructure Adoption In The Post-Covid Economy: Economic Implications Of Aws Within Tc8 Information Systems Frameworks. *American Journal of Interdisciplinary Studies*, *3*(02), 62-90. https://doi.org/10.63125/1eg7b369

[6]. Enlow, H. K., Fox, G. A., & Guertault, L. (2017). Watershed variability in streambank erodibility and implications for erosion prediction. *Water*, *9*(8), 605. https://doi.org/10.3390/w9080605

[7]. Grabowski, R. C., Droppo, I. G., & Wharton, G. (2011). Erodibility of cohesive sediment: The importance of sediment properties. *Earth-Science Reviews*, *105*(3–4), 101–120. https://doi.org/10.1016/j.earscirev.2011.01.008

[8]. Gutierrez, B. T., Plant, N. G., & Thieler, E. R. (2011). A Bayesian network to predict coastal vulnerability to sea level rise. *Journal of Geophysical Research: Earth Surface*, *116*(F2), F02024. https://doi.org/10.1029/2010jf001891

[9]. Hersbach, H., Bell, B., Berrisford, P., Hirahara, S., Horányi, A., Muñoz-Sabater, J., Nicolas, J., Peubey, C., Radu, R., Schepers, D., Simmons, A., Soci, C., Abdalla, S., Abellan, X., Balsamo, G., Bechtold, P., Biavati, G., Bidlot, J., Bonavita, M., & … Thépaut, J.-N. (2020). The ERA5 global reanalysis. *Quarterly Journal of the Royal Meteorological Society*, *146*(730), 1999–2049. https://doi.org/10.1002/qj.3803

[10]. Hinkel, J., Lincke, D., Vafeidis, A. T., Perrette, M., Nicholls, R. J., Tol, R. S. J., Marzeion, B., Fettweis, X., Ionescu, C., & Levermann, A. (2014). Coastal flood damage and adaptation costs under 21st century sea-level rise. *Proceedings of the National Academy of Sciences*, *111*(9), 3292–3297. https://doi.org/10.1073/pnas.1222469111

[11]. Holman, R. A., & Stanley, J. (2007). The history and technical capabilities of Argus. *Coastal Engineering*, *54*(6–7), 477–491. https://doi.org/10.1016/j.coastaleng.2007.01.003

[12]. Houser, C., Wernette, P., Rentschlar, E., Jones, H., Hammond, B., & Trimble, S. (2015). Post-storm beach and dune recovery: Implications for barrier island resilience. *Geomorphology*, *234*, 54–63. https://doi.org/10.1016/j.geomorph.2014.12.044

[13]. Idier, D., Castelle, B., Charles, E., & Mallet, C. (2013). Longshore sediment flux hindcast: Spatio-temporal variability along the SW Atlantic coast of France. *Journal of Coastal Research*, *65*(sp2), 1785–1790. https://doi.org/10.2112/si65-302.1

[14]. Jahid, M. K. A. S. R. (2022). Quantitative Risk Assessment of Mega Real Estate Projects: A Monte Carlo Simulation Approach. *Journal of Sustainable Development and Policy*, *1*(02), 01-34. https://doi.org/10.63125/nh269421

[15]. Karamigolbaghi, M., Ghaneeizad, S. M., Atkinson, J. F., Bennett, S. J., & Wells, R. R. (2017). Critical assessment of jet erosion test methodologies for cohesive soil and sediment. *Geomorphology*, *295*, 529–536. https://doi.org/10.1016/j.geomorph.2017.08.005

[16]. Kinnell, P. I. A. (2010). Event soil loss, runoff and the Universal Soil Loss Equation family of models: A review. *Journal of Hydrology*, *385*(1–4), 384–397. https://doi.org/10.1016/j.jhydrol.2010.01.024

[17]. Knapen, A., Poesen, J., Govers, G., Gyssels, G., & Nachtergaele, J. (2007). Resistance of soils to concentrated flow erosion: A review. *Earth-Science Reviews*, *80*(1–2), 75–109. https://doi.org/10.1016/j.earscirev.2006.10.001

[18]. Luijendijk, A., Hagenaars, G., Ranasinghe, R., Baart, F., Donchyts, G., & Aarninkhof, S. (2018). The state of the world's beaches. *Scientific Reports*, *8*, 6641. https://doi.org/10.1038/s41598-018-24630-6

[19]. Masselink, G., Castelle, B., Scott, T., Dodet, G., Suanez, S., Jackson, D., & Floc'h, F. (2016). Extreme wave activity during 2013/2014 winter and morphological impacts along the Atlantic coast of Europe. *Geophysical Research Letters*, *43*(5), 2135–2143. https://doi.org/10.1002/2015gl067492

[20]. Md Ismail, H. (2022). Deployment Of AI-Supported Structural Health Monitoring Systems For In-Service Bridges Using IoT Sensor Networks. *Journal of Sustainable Development and Policy*, *1*(04), 01-30. https://doi.org/10.63125/j3sadb56

[21]. Md Rezaul, K. (2021). Innovation Of Biodegradable Antimicrobial Fabrics For Sustainable Face Masks Production To Reduce Respiratory Disease Transmission. *International Journal of Business and Economics Insights*, *1*(4), 01–31. https://doi.org/10.63125/ba6xzq34

[22]. Md Takbir Hossen, S., & Md Atiqur, R. (2022). Advancements In 3D Printing Techniques For Polymer Fiber-Reinforced Textile Composites: A Systematic Literature Review. *American Journal of Interdisciplinary Studies*, *3*(04), 32-60. https://doi.org/10.63125/s4r5m391

[23]. Md.Kamrul, K., & Md Omar, F. (2022). Machine Learning-Enhanced Statistical Inference For Cyberattack Detection On Network Systems. *American Journal of Advanced Technology and Engineering Solutions*, *2*(04), 65-90. https://doi.org/10.63125/sw7jzx60

[24]. Muis, S., Verlaan, M., Winsemius, H. C., Aerts, J. C. J. H., & Ward, P. J. (2018). Global probabilistic projections of extreme sea levels. *Nature Communications*, *9*, 2360. https://doi.org/10.1038/s41467-018-04692-w

[25]. Narayan, S., Beck, M. W., Wilson, P., Thomas, C. J., Guerrero, A., Shepard, C. C., Reguero, B. G., Franco, G., Ingram, J. C., & Trespalacios, D. (2016). The effectiveness, costs and coastal protection benefits of natural and nature-based defences. *PLOS ONE*, *11*(5), e0154735. https://doi.org/10.1371/journal.pone.0154735

[26]. Nicholls, R. J., & Cazenave, A. (2010). Sea-level rise and its impact on coastal zones. *Science*, *328*(5985), 1517–1520. https://doi.org/10.1126/science.1185782

[27]. Panagos, P., Ballabio, C., Borrelli, P., Meusburger, K., Klik, A., Rousseva, S., Tadić, M. P., Michaelides, S., Hrabalíková, M., Olsen, P., Aalto, J., Lakatos, M., Rymszewicz, A., Dumitrescu, A., Beguería, S., & Alewell, C. (2017). Global rainfall erosivity assessment based on high-temporal resolution rainfall records. *Scientific Reports*, *7*, 4175. https://doi.org/10.1038/s41598-017-04282-8

[28]. Pardo-Pascual, J. E., Almonacid-Caballer, J., Ruiz, L. A., & Palomar-Vázquez, J. (2012). Automatic extraction of shorelines from Landsat TM and ETM+ multi-temporal images with subpixel precision. *Remote Sensing of Environment*, *123*, 1–11. https://doi.org/10.1016/j.rse.2012.02.024

[29]. Plant, N. G., Stockdon, H. F., Sallenger, A. H., Jr., Holman, R. A., & Holland, K. T. (2009). A probabilistic formulation of nearshore processes for shoreline prediction. *Journal of Geophysical Research: Earth Surface*, *114*(F3), F03015. https://doi.org/10.1029/2008jf001123

[30]. Ranasinghe, R. (2016). Assessing climate change impacts on open sandy coasts: A review. *Earth-Science Reviews*, *160*, 320–332. https://doi.org/10.1016/j.earscirev.2016.07.011

[31]. Razia, S. (2022). A Review Of Data-Driven Communication In Economic Recovery: Implications Of ICT-Enabled Strategies For Human Resource Engagement. *International Journal of Business and Economics Insights*, *2*(1), 01-34. https://doi.org/10.63125/7tkv8v34

[32]. Ruggiero, P. (2013). Is the intensifying Pacific storm track contributing to rising coastal inundation hazards? *Oceanography*, *26*(4), 68–79. https://doi.org/10.5670/oceanog.2013.93

[33]. Ruggiero, P., Komar, P. D., & Allan, J. C. (2010). Increasing wave heights and extreme value analyses along the U.S. Pacific Northwest coast. *Coastal Engineering*, *57*(2), 539–552. https://doi.org/10.1016/j.coastaleng.2009.12.005

[34]. Sadia, T. (2022). Quantitative Structure-Activity Relationship (QSAR) Modeling of Bioactive Compounds From Mangifera Indica For Anti-Diabetic Drug Development. *American Journal of Advanced Technology and Engineering Solutions*, *2*(02), 01-32. https://doi.org/10.63125/ffkez356

[35]. Shepard, C. C., Crain, C. M., & Beck, M. W. (2011). The protective role of coastal marshes: A systematic review and meta-analysis. *PLOS ONE*, *6*(11), e27374. https://doi.org/10.1371/journal.pone.0027374

[36]. Slott, J. M., Murray, A. B., Ashton, A. D., & Crowley, T. J. (2006). Coastline responses to changing storm patterns. *Geophysical Research Letters*, *33*(18), L18404. https://doi.org/10.1029/2006gl027445

[37]. Smit, B., & Wandel, J. (2006). Adaptation, adaptive capacity and vulnerability. *Global Environmental Change*, *16*(3), 282–292. https://doi.org/10.1016/j.gloenvcha.2006.03.008

[38]. Splinter, K. D., Turner, I. L., & Davidson, M. A. (2014). A generalized equilibrium model for predicting daily to interannual shoreline response. *Journal of Geophysical Research: Earth Surface*, *119*(9), 1936–1958. https://doi.org/10.1002/2013jf002750

[39]. Stevenson, S., Fowler, H. J., Lenderink, G., & Verkade, J. (2019). Rainfall intensity bursts and the erosion of soils: An analysis of short-duration extremes. *Earth Surface Dynamics*, *7*(2), 345–365. https://doi.org/10.5194/esurf-7-345-2019

[40]. Stockdon, H. F., Holman, R. A., Howd, P. A., & Sallenger, A. H., Jr. (2006). Empirical parameterization of setup, swash, and runup. *Coastal Engineering*, *53*(7), 573–588. https://doi.org/10.1016/j.coastaleng.2006.07.005

[41]. Temmerman, S., Meire, P., Bouma, T. J., Herman, P. M. J., Ysebaert, T., & de Vriend, H. J. (2013). Ecosystem-based coastal defence in the face of global change. *Nature*, *504*(7478), 79–83. https://doi.org/10.1038/nature12859

[42]. Turner, I. L., Harley, M. D., & Drummond, C. D. (2016). UAVs for coastal surveying. *Coastal Engineering*, *114*, 19–24. https://doi.org/10.1016/j.coastaleng.2016.03.011

[43]. Vitousek, S., Barnard, P. L., Fletcher, C. H., Frazer, N., Erikson, L., & Storlazzi, C. D. (2017). Doubling of coastal flooding frequency within decades due to sea-level rise: Implications for coastal engineering and management. *Scientific Reports*, *7*, 1399. https://doi.org/10.1038/s41598-017-03364-6

[44]. Vousdoukas, M. I., Ranasinghe, R., Mentaschi, L., Plomaritis, T. A., Athanasiou, P., Luijendijk, A., & Feyen, L. (2020). Sandy coastlines under threat of erosion. *Nature Climate Change*, *10*(3), 260–263. https://doi.org/10.1038/s41558-020-0697-0

[45]. Westoby, M. J., Brasington, J., Glasser, N. F., Hambrey, M. J., & Reynolds, J. M. (2012). "Structure-from-Motion" photogrammetry: A low-cost, effective tool for geoscience applications. *Geomorphology*, *179*, 300–314. https://doi.org/10.1016/j.geomorph.2012.08.021

[46]. Young, A. P., Guza, R. T., O'Reilly, W. C., Flick, R. E., & Gutierrez, R. (2011). Short-term retreat statistics of a slowly eroding coastal cliff. *Natural Hazards and Earth System Sciences*, *11*(1), 205–217. https://doi.org/10.5194/nhess-11-205-2011

[47]. Young, I. R., Zieger, S., & Babanin, A. V. (2011). Global trends in wind speed and wave height. *Science*, *332*(6028), 451–455. https://doi.org/10.1126/science.1197219